Supplementary Information

Azido-enabled thermal history analysis on metal-oxide surface

Satoki Yamaguchi, Tomohiro Iwai,* Hiromichi V. Miyagishi, Hiroshi Masai, Takuro Hosomi, Takeshi Yanagida, Ken Uchida and Jun Terao*

E-mail: ciwai@g.ecc.u-tokyo.ac.jp (T.I.), cterao@g.ecc.u-tokyo.ac.jp (J.T.)

1. Materials

Unless otherwise noted, manipulations for organic synthesis were performed under nitrogen atmosphere using standard Schlenk-type glassware in a dual-manifold Schlenk line. Unless otherwise stated, commercially available chemicals were used as received. Dehydrated toluene, tetrahydrofuran, dichloromethane, and *N,N*-dimethylformamide (DMF) were purchased from KANTO CHEMICAL Co., Inc., and further purified by passage through activated alumina under positive nitrogen pressure as described by Grubbs *et al*.[1] Si(100) substrates (double side polished, 700–800 Ω, n-type) for ZnO nanowires (NWs) fabrication were purchased. Si(100) substrates with SiO_2 layer (300 nm) were purchased from S.E.H. Silicon Wafers.

2. Experimental equipment

***NMR spectroscopy*:** ^{1}H NMR (500 MHz), ^{13}C {^{1}H} NMR (126 MHz), and ^{31}P{^{1}H} NMR (202 MHz) spectra were measured with a Bruker AVANCE-500 spectrometer. The ^{1}H NMR chemical shifts are reported relative to tetramethylsilane (0.00 ppm), or residual protonated solvents in dimethyl sulfoxide-d_6 (DMSO, 2.54 ppm). The ^{13}C NMR chemical shifts are reported relative to deuterated solvents ($CDCl_3$, 77.16 ppm or DMSO-d_6, 41.23 ppm). The ^{31}P NMR spectra were also recorded using 85% H_3PO_4 as an external standard.

***High-resolution mass spectroscopy (HR-MS)*:** Electrospray ionization time-of-flight (ESI-ToF) mass spectra were obtained using a Bruker micrOTOF II-KE02. The HR-MS spectra were internally calibrated using sodium trifluoroacetate cluster ions. Atmospheric Pressure Chemical Ionization (APCI)-orbitrap-MS was obtained using a Thermo Fisher Scientific Exactive Plus in Mass Spectrometry Room in Graduate School of Engineering, Kyoto University.

***Preparative recycling gel permeation chromatography (GPC)*:** Preparative recycling GPC was performed with a JAI LaboACE LC-5060 equipped with JAIGEL-1HH column, using $CHCl_3$ as the eluent at flow rate of 7.5 mL min^{-1}, a JAI LaboACE LC-5060 PlusII equipped with JAIGEL-1HH column, using $CHCl_3$ as the eluent at flow rate of 7.5 mL min^{-1}, or a JAI LaboACE LC-5060 PlusII equipped with JAIGEL-1H column, using $CHCl_3$ as the eluent at flow rate of 14 mL min^{-1}.

Thermogravimetric analysis (TG): TG was conducted with a Thermo Plus 2 thermogravimetric analyzer (Rigaku) with α-Al_2O_3 as a reference.

Fourier transform infrared spectroscopy (FT-IR): The FT-IR spectra were recorded on a Thermo Fisher Scientific Nicolet iS50 FT-IR spectrometer equipped with a mercury-cadmium-telluride detector. The test room was constantly purged with dry air. The FT-IR spectra of the surface molecules immobilized on the ZnO NWs were recorded at room temperature. 300 scans

were accumulated to obtain each spectrum with a resolution of 4 cm^{-1}. FT-IR spectra of bare ZnO NWs were used as the background spectrum for the other measurements.

Scanning electron microscopy-energy dispersive X-ray spectrometry (SEM-EDS)*:* Scanning electron microscope (SEM) images equipped with EDS were acquired using a JEOL JSM-7610F.

Laser lithography: Laser lithography was performed with Heidelberg Instruments μPG 101 UOW1 at an energy of 40 mW.

Sputtering: Radio Frequency (RF) sputtering (Seinan, order-made) was used.

UV-O_3 cleaner: UV ozone cleaning was performed using UV Ozone Cleaner UV-1 (SAMCO).

Flash column chromatography: Flash column chromatography was performed using Isolera One (Biotage).

3. Synthetic procedures of 1 and 2

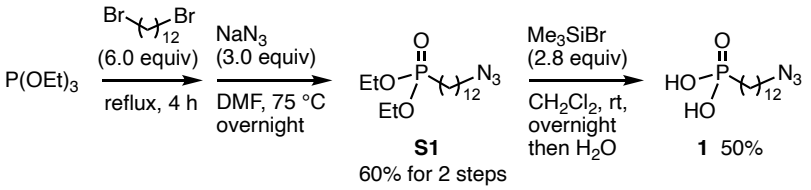

Scheme S1 Synthetic routes to **1**.

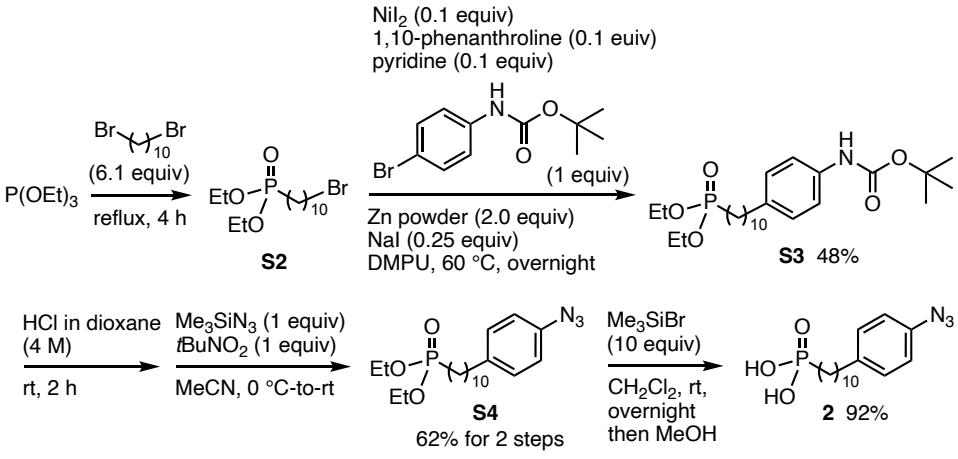

Scheme S2 Synthetic routes to **2**.

[Compound S1]

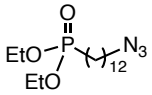

A mixture of triethylphosphite (2.00 mL, 11.6 mmol) and 1,12-dibromododecane (22.9 g, 69.8 mmol, 6.0 equiv) was heated under reflux for 4 h. The excess 1,12-dibromododecane was removed by distillation, and then the crude product was further purified by silica gel column chromatography (*n*-hexane/ethyl acetate 3:1 to 1:1). The resulting product was used for the next reaction without further purification.

A solution of the product (3.07 g, 7.97 mmol) and sodium azide (1.58 g, 24.3 mmol, 3.0 equiv) in dehydrated DMF (80 mL) was stirred overnight at 75 °C. After cooling to room temperature, brine (80 mL) was added. The mixture was extracted with ethyl acetate (3 times). The combined organic layers were washed with brine (5 times) and then concentrated to give **S1** as a pale yellow oil (2.41 g, 6.95 mmol, 60% yield for 2 steps).

^{1}H NMR ($CDCl_3$, 500 MHz): δ 4.13–4.05 (m, 4H, -O-C$\underline{H}_2$-), 3.26 (t, J = 7.0 Hz, 2H, N_3-C$\underline{H}_2$-), 1.75–1.68 (m, 2H, P-C$\underline{H}_2$-), 1.65–1.55 (m, 4H, N_3-CH_2-C$\underline{H}_2$- and P-CH_2-C$\underline{H}_2$-), 1.38–1.27 (m, 22H, -C$\underline{H}_2$- and -O-CH_2-C$\underline{H}_3$). The ^{1}H NMR spectrum was consistent with those previously reported (Fig. S22).[2]

[Compound 1]

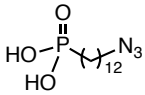

A solution of **S1** (844 μL, 3.47 mmol) and trimethylsilyl bromide (1.24 mL, 9.53 mmol, 2.8 equiv) in dehydrated dichloromethane was stirred under nitrogen atmosphere overnight at room temperature. After removal of volatiles under vacuum, water (8 mL) was added, and the mixture was stirred overnight at room temperature. The resulting white solid was filtered and dried under vacuum to give **1** as a white solid (506 mg, 1.74 mmol, 50% yield).

^{1}H NMR ($CDCl_3$, 500 MHz): δ 3.26 (t, J = 7.0 Hz, 2H, N_3-C$\underline{H}_2$-), 1.79–1.72 (m, 2H, P-C$\underline{H}_2$-), 1.64–1.57 (m, 4H, N_3-CH_2-C$\underline{H}_2$- and P-CH_2-C$\underline{H}_2$-), 1.38–1.27 (m, 16H). The ^{1}H NMR spectrum was consistent with those previously reported (Fig. S23).[2]

[Compound S2]

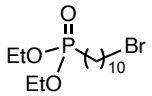

A mixture of triethylphosphite (2.17 mL, 12.5 mmol) and 1,10-dibromodecane (22.9 g, 76.4 mmol, 6.1 equiv) was heated under reflux for 4 h. The excess 1,10-dibromodecane was distilled off under vacuum, and then the crude product was purified by silica gel column chromatography (*n*-hexane/ethyl acetate 1:1) to give **S2** as an orange oil (1.86 g, 5.21 mmol, 42% yield).

^{1}H NMR ($CDCl_3$, 500 MHz): δ 4.15–4.03 (m, 4H, -O-C$\underline{H}_2$-), 3.41 (t, J = 6.9 Hz, 2H, Br-C$\underline{H}_2$-), 1.88–1.82 (m, 2H, Br-CH$_2$-C$\underline{H}_2$-), 1.75–1.68 (m, 2H, P-C$\underline{H}_2$-), 1.64–1.55 (m, 2H, P-CH$_2$-C$\underline{H}_2$-), 1.46–1.28 (m, 18H, -C$\underline{H}_2$- and -O-CH$_2$-C$\underline{H}_3$). The ^{1}H NMR spectrum was consistent with those previously reported (Fig. S24).[3]

[Compound S3]

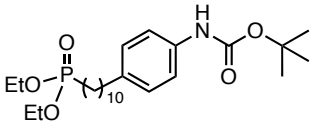

A mixture of **S2** (625 μL, 2.80 mmol), *tert*-butyl (4-bromophenyl)carbamate (763 mg, 2.80 mmol, 1.0 equiv), Zn powder (367 mg, 5.61 mmol, 2.0 equiv), NaI (105 mg, 0.698 mol, 0.25 equiv), NiI_2 (89.4 mg, 0.286 mmol, 0.10 equiv), 1,10-phenanthroline (50.8 mg, 0.282 mmol, 0.10 equiv), and pyridine (22.6 μL, 0.282 mmol, 0.10 equiv) in *N*,*N*'-dimethylpropyleneurea (DMPU, 40 mL) degassed with N_2 bubbling was stirred under nitrogen atmosphere overnight at 60 °C. After cooling to room temperature, Zn powder was removed by filtration. *n*-Hexane and ethyl acetate were added to the filtrate, and the mixture was washed with water (3 times). The organic layer was dried over $MgSO_4$, filtered, and evaporated under vacuum. The residue was purified by silica gel column chromatography (*n*-hexane/ethyl acetate 3:1) followed by GPC with chloroform as the eluent to give **S3** as a yellow oil (629 mg, 1.34 mmol, 48% yield).

^{1}H NMR ($CDCl_3$, 500 MHz): δ 7.28 (d, J = 8.0 Hz, 2H, ArH), 7.07 (d, J = 8.5 Hz, 2H, ArH), 6.85 (s, 1H, Ar-N$\underline{H}$-), 4.13–4.04 (m, 4H, -O-C$\underline{H}_2$-), 2.53 (t, J = 7.7 Hz, 2H, Ar-C$\underline{H}_2$-), 1.75–1.68 (m, 2H, P-C$\underline{H}_2$-), 1.63–1.51 (m, 13H, Ar-CH$_2$-C$\underline{H}_2$-, P-CH$_2$-C$\underline{H}_2$-, and –C(C$\underline{H}_3$)$_3$), 1.38–1.25 (m, 18H, -C$\underline{H}_2$- and -O-CH$_2$-C$\underline{H}_3$) (Fig. S25).

^{13}C NMR ($CDCl_3$, 126 MHz): δ 153.06, 137.43, 136.14, 128.73, 118.72, 80.04, 61.36 (d, J = 6.6 Hz), 35.21, 31.52, 30.59 (d, J = 17.1 Hz), 29.47, 29.42, 29.32, 29.13, 29.06, 28.38, 25.68 (d, J = 140.6 Hz), 22.38 (d, J = 5.4 Hz), 16.48 (d, J = 5.9 Hz) (Fig. S26).

^{31}P NMR ($CDCl_3$, 202 MHz): δ 33.15 (Fig. S27).

HR-MS (ESI-ToF-MS) *m*/*z*: [**S3**+Na]$^+$ calcd for $C_{25}H_{44}NO_5PNa$ 492.2849, found 492.2858.

[Compound S4]

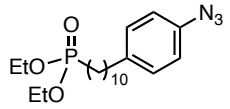

A solution of **S3** (321 mg, 0.683 mmol) in HCl in dioxane (4 M, 3.2 mL) was stirred for 2 h at room temperature. After quenching with $NaHCO_3$ aq., and the resulting mixture was extracted with ethyl acetate (3 times). The combined organic layers were dried over $MgSO_4$, filtered, and evaporated in vacuum. The crude product was used for the next reaction without further purification.

To a solution of the product (190 mg, 0.514 mmol) in dehydrated acetonitrile (6 mL), trimetylsilyl azide (673 μL, 5.14 mmol, 10 equiv) and *tert*-butyl nitrite (609 μL, 5.14 mmol, 10 equiv) were sequentially added dropwise under nitrogen atmosphere at 0 °C. The solution was stirred at 0 °C for 30 min and then allowed to warm to room temperature and stirred for an additional 4 h. After removal of volatiles under vacuum, the residue was purified by GPC with chloroform as the eluent to give **S4** as a yellow oil (145 mg, 0.366 mmol, 62% yield for 2 steps).

^{1}H NMR ($CDCl_3$, 500 MHz): δ 7.15 (d, J = 8.4 Hz, 2H, ArH), 6.94 (d, J = 8.5 Hz, 2H, ArH), 4.13–4.05 (m, 4H, -O-C$\underline{H}_2$-), 2.57 (t, J = 7.7 Hz, 2H, Ar-C$\underline{H}_2$-), 1.75–1.68 (m, 2H, P-C$\underline{H}_2$-), 1.63–1.54 (m, 4H, Ar-CH$_2$-C$\underline{H}_2$- and P-CH$_2$-C$\underline{H}_2$-), 1.37–1.26 (m, 18H, -C$\underline{H}_2$- and -O-CH$_2$-C$\underline{H}_3$) (Fig. S28).

^{13}C NMR ($CDCl_3$, 126 MHz): δ 139.86, 137.39, 129.82, 118.96, 61.51 (d, J = 6.3 Hz), 35.42, 31.60, 30.72 (d, J = 17.1 Hz), 29.61, 29.55, 29.47, 29.30, 29.20, 25.82 (d, J = 140.5 Hz), 22.52 (d, J = 5.5 Hz), 16.61 (d, J = 5.9 Hz) (Fig. S29).

^{31}P NMR ($CDCl_3$, 202 MHz): δ 33.20 (Fig. S30).

HR-MS (ESI-ToF-MS) m/z: [**S4**+Na]$^+$ calcd for $C_{20}H_{34}NO_3PNa$ 418.2230, found 418.2259.

[Compound 2]

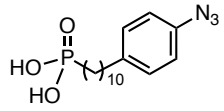

A solution of **S4** (127 mg, 0.321 mmol) and trimethylsilyl bromide (416 μL, 3.21 mmol, 10 equiv) in dehydrated dichloromethane (5 mL) was stirred under N_2 atmosphere overnight at room temperature. After removal of volatiles under vacuum, MeOH (5 mL) was added, and the resulting mixture was stirred overnight at room temperature. After removal of volatiles under vacuum, 1 M HCl aq. was added. The mixture was extracted with chloroform (3 times). The

combined organic layers were dried over $MgSO_4$, filtered, and evaporated under vacuum to give **2** as a yellow solid (100 mg, 0.296 mmol, 92% yield).

^{1}H NMR (DMSO-d_6, 500 MHz): δ 7.22 (d, J = 8.4 Hz, 2H, ArH), 7.01 (d, J = 8.5 Hz, 2H, ArH), 2.54 (t, J = 7.7 Hz, 2H, Ar-C$\underline{H}_2$-), 1.55–1.50 (m, 2H, P-C$\underline{H}_2$-), 1.48–1.39 (m, 4H, Ar-CH$_2$-C$\underline{H}_2$- and P-CH$_2$-C$\underline{H}_2$-), 1.29–1.22 (m, 12H, -C$\underline{H}_2$- and -O-CH$_2$-C$\underline{H}_3$) (Fig. S31).

^{13}C NMR (DMSO-d_6, 126 MHz): δ 141.16, 138.35, 131.54, 120.63, 36.15, 32.67, 31.86 (d, J = 15.8 Hz), 30.70, 30.59, 30.56, 30.43, 30.28, 29.52 (d, J = 136.5 Hz), 24.57 (d, J = 4.7 Hz) (Fig. S32).

^{31}P NMR (DMSO-d_6, 202 MHz): δ 26.74 (Fig. S33).

HR-MS (APCI-MS) m/z: [**S4**–H]$^-$ calcd for $C_{16}H_{25}N_3O_3P$ 338.1639, found 338.1649.

4. Synthetic procedures of molecular probes for SEM-EDS analysis

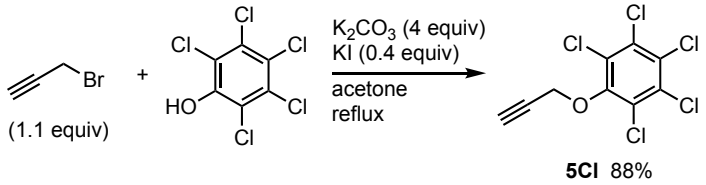

Scheme S3 Synthetic routes to **5Cl**.

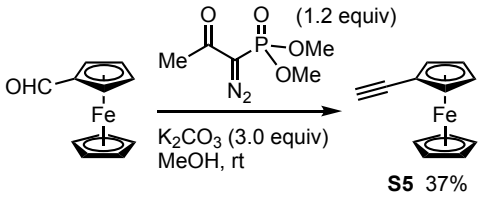

Scheme S4 Synthetic routes to **S5**.

[Compound 5Cl]

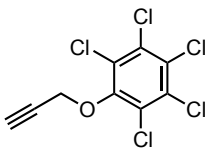

To a mixture of pentachlorophenol (1.01 g, 3.75 mmol), KI (252 mg, 1.51 mmol, 0.40 equiv) and K_2CO_3 (2.05 g, 15.0 mmol, 4.0 equiv) in dried acetone (45 mL) was added 3-bromo-1-propyne (449 μL, 9.2 M in toluene, 1.1 equiv). The mixture was refluxed under nitrogen atmosphere overnight. After cooling to room temperature, the crude product was purified by flash column chromatography with *n*-hexane as the eluent to give **5Cl** as a white solid (1.01 g, 3.32 mmol, 88% yield).

^{1}H NMR ($CDCl_3$, 500 MHz): δ 4.82 (d, *J* = 2.5 Hz, 2H, C<u>H</u>$_2$), 2.58 (t, *J* = 2.5 Hz, 1H, CC<u>H</u>). The ^{1}H NMR spectrum was consistent with those previously reported (Fig. S34).[4]

[Compound S5]

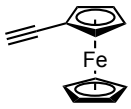

To a mixture of ferrocenecarboxaldehyde (997 mg, 4.66 mmol), K_2CO_3 and (1.93 g, 14.0 mmol, 3.0 equiv) in dried MeOH (60 mL), dimethyl (1-diazo-2-oxopropyl)phoshonate (841 μL, 5.61 mmol, 1.2 equiv) was added. The mixture was stirred at room temperature under nitrogen atmosphere overnight. After quenching by addition of water (~200 mL), the resulting mixture was extracted with *n*-hexane (3 times). The combined organic layer was dried over $MgSO_4$, filtered, and evaporated under vacuum. The residue was purified by silica gel column chromatography with *n*-hexane as the eluent to give **S5** as a red oil (366 mg, 1.72 mmol, 37% yield).

^{1}H NMR ($CDCl_3$, 500 MHz): δ 4.46 (t, *J* = 1.9 Hz, 2H), 4.21 (s, 5H), 4.19 (t, *J* = 1.9 Hz, 2H), 2.71 (s, 1H, -CC<u>H</u>). The ^{1}H NMR spectrum was consistent with those previously reported (Fig. S35).[5]

5. TG analysis of organic azides

TG analysis of **1** and **2** was conducted under a dry N_2 flow (100 mL min^{-1}) in the temperature range of 30–400 °C and an increasing rate of 5 K min^{-1} for both **1** and **2** (Fig. S1).

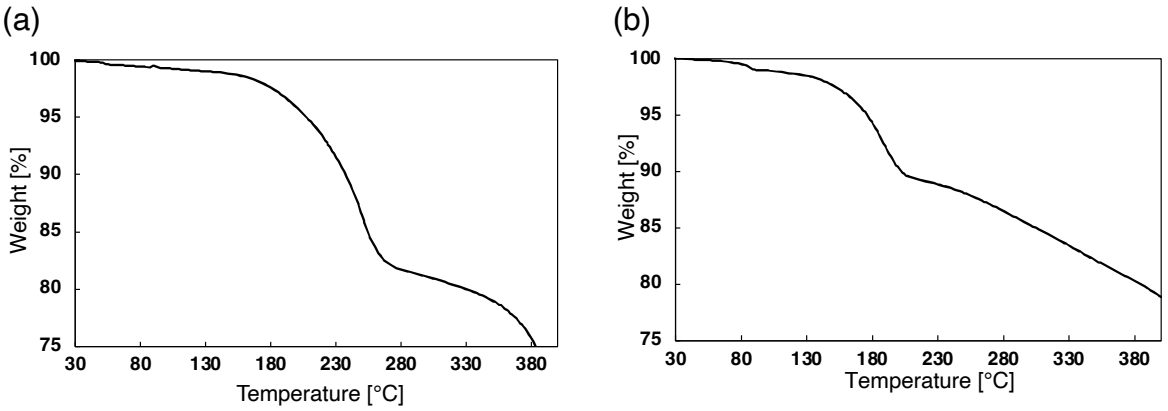

Fig. S1 TG curve of (a) **1** and (b) **2** recorded in the temperature range 30–400 °C (increasing rate = 5 K min^{-1} under N_2 in 100 mL min^{-1} stream).

6. Surface Modification on ZnO nanowire arrays and characterization

6.1. Procedure of ZnO nanowires grown on a Si substrate: ZnO NWs on Si(100) wafers were grown using the hydrothermal method (Fig. S2a).[6] A solution of 0.30 M $Zn(OAc)_2 \cdot 2H_2O$ and 0.50 M 2-ethanolamine in dehydrated ethanol (5 mL) was heated at 60 °C for 1 h. Then, 300 μL of the solution was dropped on a UV-O_3 cleaned Si(100) wafer (2 cm×2 cm), to conduct spin coat (500 rpm 5 s→3000 rpm 60 s). The samples were annealed at 400 °C in the air for 1 h. Meanwhile, 5.5 mM polyethylenimine (Mw ~2,000, 50 wt.% in H_2O), 25 mM hexamethylenetetramine, and 25 mM $Zn(NO_3)_2 \cdot 6H_2O$ were dissolved sequentially in distilled water (200 mL). The pre-prepared substrate was dipped into the solution and maintained at 80 °C for 16 h. After cooling to room temperature, the samples were rinsed with distilled water. Then the as-grown ZnO NWs were annealed at 400 °C in the air for 1 h. The SEM analysis confirm that the ZnO NWs grew as hexagonal columnar structures (Fig. S2b).

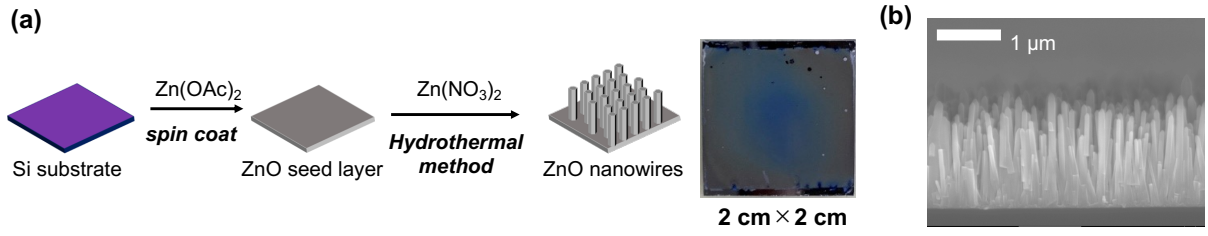

Fig. S2 (a) Schematic procedure and photographic images of ZnO nanowire arrays. (b) The side view of the array observed by SEM analysis.

6.2. Surface modification of ZnO nanowires: Modification solutions (0.24 μM) were prepared by dissolving the azide **1** or **2** in toluene at room temperature. The ZnO nanowire array on Si wafers was dipped into the solution (10 mL) for 30 min at room temperature. Then, the samples were washed several times with toluene and dried under N_2 flow. The modified ZnO nanowires are characterized by FT-IR spectroscopies (Fig. S3).

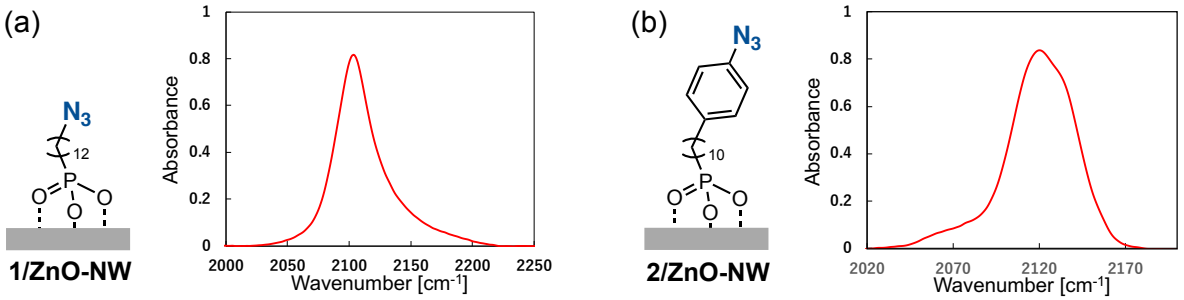

Fig. S3 Structure and FT-IR spectra of azide region of (a) **1/ZnO-NW** and (b) **2/ZnO-NW**.

6.3. FT-IR analysis of azido-functionalized ZnO nanowires heated on a hotplate: To precisely control the heating temperature, **1/ZnO-NW** or **2/ZnO-NW** placed on a copper plate were covered with aluminum foil and then heated on a hotplate (Fig. S4). The heating temperature was measured using a thermocouple connected to the copper plate. The temperature difference was within 2 °C.

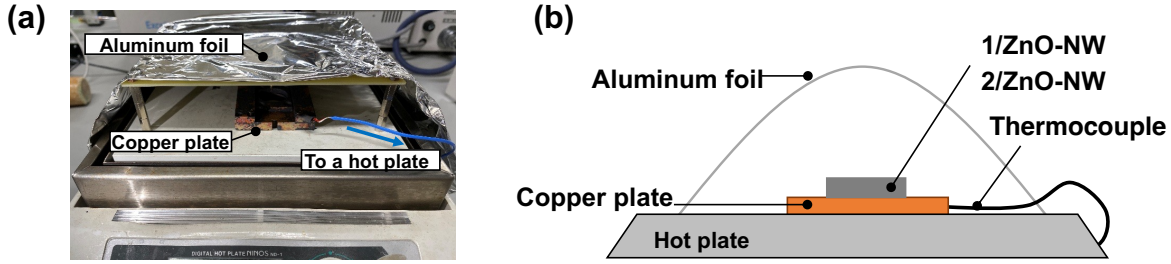

Fig. S4 (a) Photo and (b) graphical images of the heating system using a hotplate.

The azide pyrolysis of **1/ZnO-NW** (at 200, 220, and 235 °C) and **2/ZnO-NW** (at 150, 160, and 170 °C) were monitored by FT-IR analysis (Fig. S5 and S6). The relationship between reaction rate constant (k) and heating temperature (T) is shown by the Arrhenius equation as follows (eqn. S1):

$$k = A \exp(-\frac{E_a}{RT}) \qquad \text{(S1)}$$

where E_a is the activation energy, R is the universal gas constant, and A is the pre-exponential coefficient. Arrhenius plot constructed from these reaction rate constants showed that the pyrolysis activation energy of the surface azido group of **1/ZnO-NW** or **2/ZnO-NW** was 147 or 155 kJ mol^{-1}, respectively.

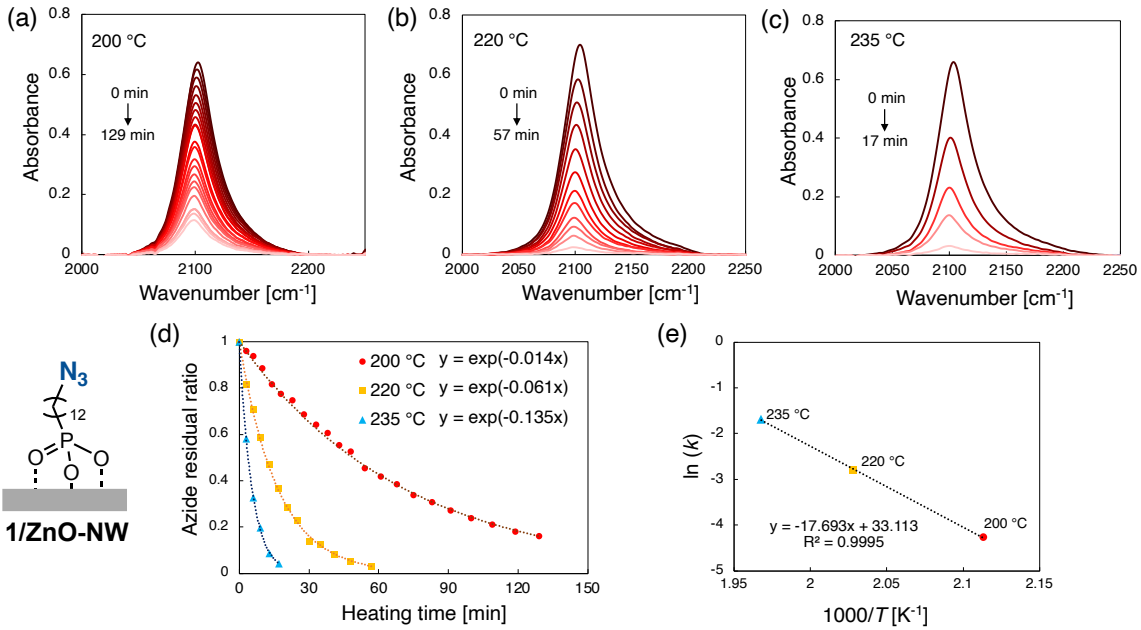

Fig. S5 FT-IR spectral changes in the azido region on **1/ZnO-NW** uniformly heated (a) at 200 °C (heating time: 0, 3, 6, 10, 14, 18, 23, 28, 33, 38, 43, 48, 54, 61, 68, 75, 83, 91, 100, 109, 119, and 129 min), (b) at 220 °C (heating time: 0, 3, 6, 9, 13, 17, 21, 25, 30, 35, 41, 48, and 57 min), and (c) at 235 °C (heating time: 0, 3, 6, 9, 13, and 17 min). (d) Time-dependent decomposition rate of the surface azido group normalized to initial amounts (red circles for 200 °C, yellow squares for 220 °C, and blue triangles for 235 °C). (d) Arrhenius plot constructed from rate constants of the surface azide pyrolysis.

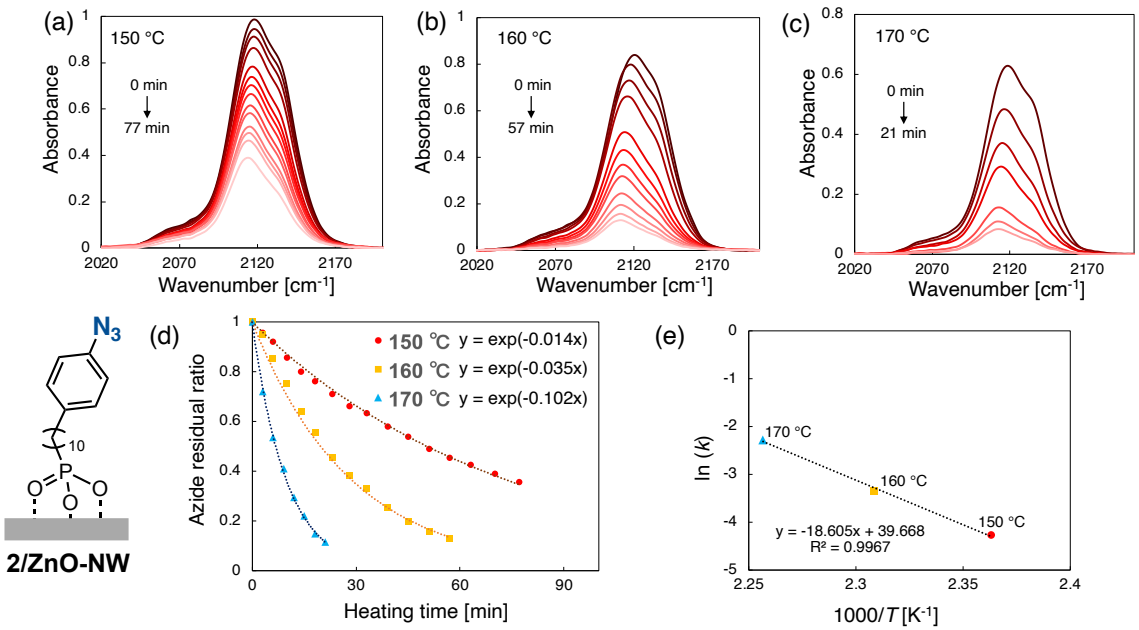

Fig. S6 FT-IR spectral changes in the azido region on **2/ZnO-NW** uniformly heated (a) at 150 °C (heating time: 0, 3, 6, 10, 14, 18, 23, 28, 33, 39, 45, 51, 57, 63, 70, and 77 min), (b) at 160 °C (heating time: 0, 3, 6, 10, 14, 18, 23, 28, 33, 39, 45, 51, and 57 min), and (c) at 170 °C (heating time: 0, 3, 6, 9, 12, 15, 18, and 21 min). (d) Time-dependent decomposition rate of the surface azido group normalized to initial amounts (red circles for 150 °C, yellow squares for 160 °C, and blue triangles for 170 °C). (d) Arrhenius plot constructed from rate constants of the surface azide pyrolysis.

6.4. Surface Huisgen cycloaddition on ZnO nanowires: A reaction mixture for surface Huisgen cycloaddition was prepared by dissolving 3.0 mM each of sodium *L*-ascorbate, $CuSO_4$, **5Cl** and 6.0 mM of tris[(1-benzyl-1*H*-1,2,3-triazol-4-yl)methyl]amine (TBTA) into 10 mL of DMSO/H_2O (9:1). The modified ZnO nanowire arrays on Si wafers (**1/ZnO-NW** or **2/ZnO-NW**) were dipped into the solution at room temperature for 30 min under air. The samples were washed with DMSO and THF, and then used for SEM-EDS analysis.

6.5. SEM-EDS analysis on ZnO nanowires: The SEM-EDS analysis was conducted in the 3 μm × 4 μm range of the substrate (accelerating voltage 15 kV). Considering the possibility of physical adsorption of **5Cl** onto the substrate, all SEM-EDS spectra were baseline corrected using substrates in which 1-dodecylphosphonic acid-modified ZnO NWs were treated under conditions of the Huisgen cycloaddition reaction with **5Cl**. The SEM-EDS values are normalized by those of the sample obtained by the Huisgen cycloaddition reaction on the non-heated azido-modified ZnO NWs.

All SEM-EDS data analysis was performed using Python program with the Numpy and JEOL_eds modules as follows.[7,8] After importing the EDS data with JEOL_eds, the EDS spectrum for the entire field of view was obtained. The baseline of the continuous X-ray background was determined by fitting a sixth-order polynomial within the energy ranges of 1.25–1.60 keV, 2.13–2.52 keV, and 2.72–4.00 keV, followed by baseline subtraction. The integrated values within the range of 2.52–2.72 keV were used for Cl, and those within 1.93–2.13 keV were used for P.

6.6. Molecular probes for SEM-EDS analysis: Fig S7a shows the SEM-EDS spectrum of **5Cl-1/ZnO-NW**, which was prepared via the Huisgen cycloaddition between non-heated **1/ZnO-NW** and **5Cl**. When ethynyl ferrocene (**S5**) was used as a probe for Fe, the resulting **S5-1/ZnO-NW** afforded independent signal around 6.3 keV, but its intensity was low (Fig S7b).

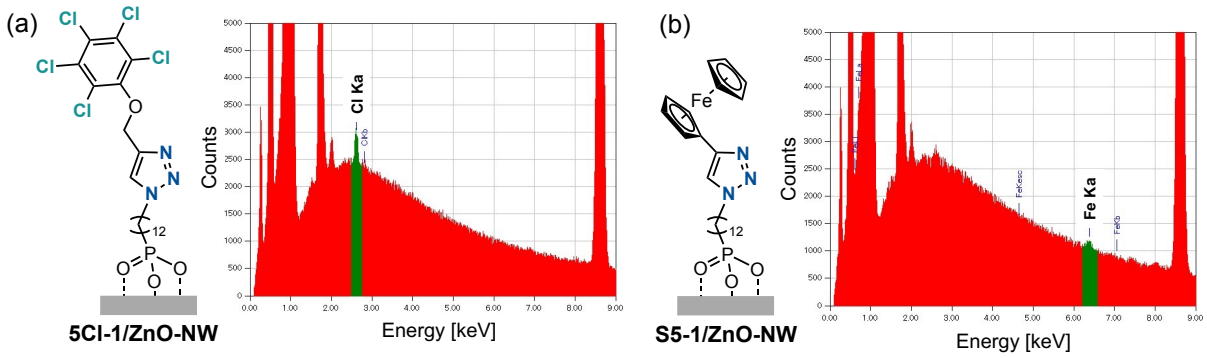

Fig. S7 SEM-EDS spectra of (a) **5Cl-1/ZnO-NW** and (b) **S5-1/ZnO-NW**.

FT-IR spectrum of **5Cl-1/ZnO-NW** shows that 35% of the azido groups remaining unconsumed after the Huisgen cycloaddition (Fig. S8). The incomplete azido conversion is probably due to the close proximity of the surface azido group, as previously reported in literatures.[9] However, this did not directly affect the present thermal history analysis.

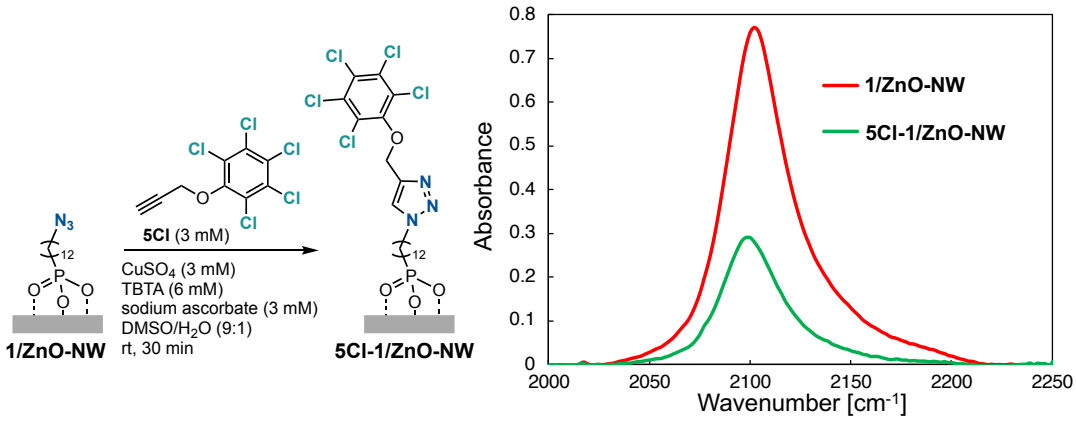

Fig. S8 FT-IR spectra of **1/ZnO-NW** and **5Cl-1/ZnO-NW**.

6.7. SEM-EDS spectral change depending on heating time using 1/ZnO-NW: 1/ZnO-NW was heated at 220 °C for 0, 10, 20, 30, 40, 50, and 60 min on a hotplate. After cooling to room temperature, **5Cl** was introduced to **1'/ZnO-NW** via Huisgen cycloaddition using the same procedure described in Section 6.4. The resulting samples, **5Cl-1'/ZnO-NW**, were used for SEM-EDS analysis (Fig. S9).

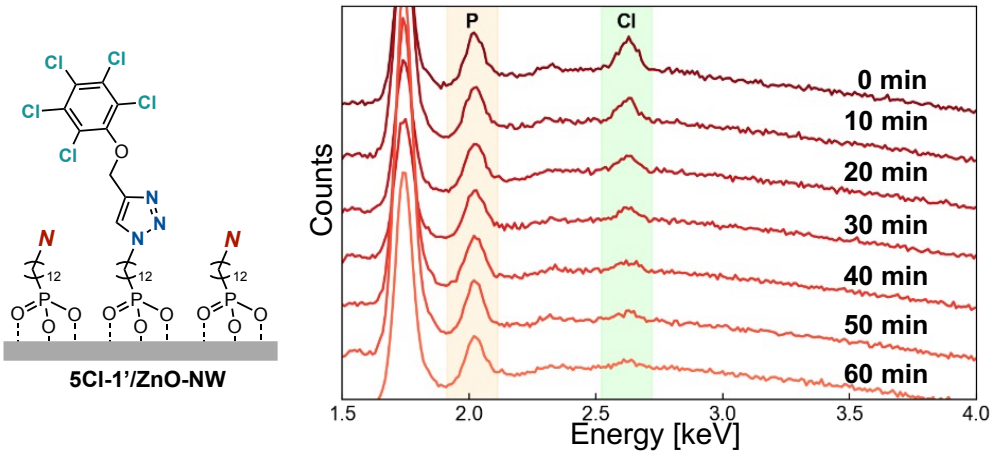

Fig. S9 SEM-EDS spectral variation of **5Cl-1'/ZnO-NW** depending on heating time (220 °C; 0, 10, 20, 30, 40, 50, and 60 min).

6.8. SEM-EDS spectral change depending on heating temperature using 1/ZnO-NW: 1/ZnO-NW was heated at 180, 190, 200, 210, 220, 230, 235, 240, 250, and 260 °C for 10 min with a hotplate. After cooling to room temperature, **5Cl** was introduced to **1'/ZnO-NW** via Huisgen cycloaddition using the same procedure described in Section 6.4. The resulting samples, **5Cl-1'/ZnO-NW**, were used for SEM-EDS analysis. The relative ratio of Cl signal intensity to P signal intensity is denoted as *Cl*/*P*. The plot of the normalized values relative to the initial level at each temperature $(Cl/P)/(Cl/P)_0$ is shown in Fig. S10.

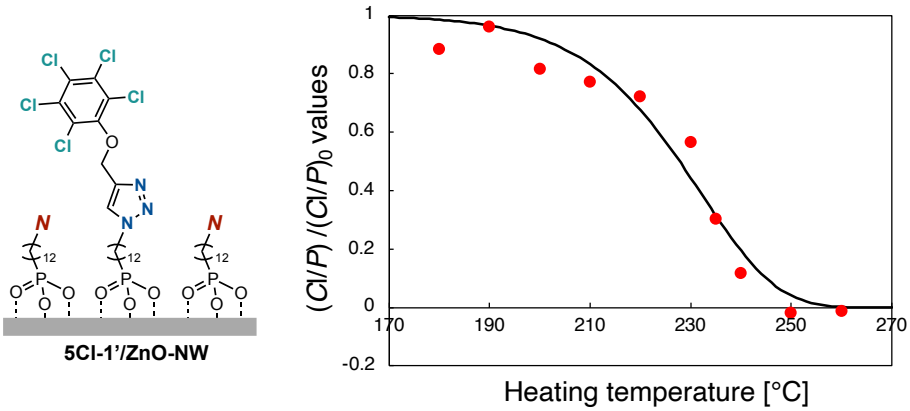

Fig. S10 Calibration curve obtained by fitting the measured $(Cl/P)/(Cl/P)_0$ values of **5Cl-1'/ZnO-NW**, based on SEM-EDS analysis (heating temperature: 180, 190, 200, 210, 220, 230, 235, 240, 250, and 260 °C for 10 min).

6.9. SEM-EDS spectral change depending on heating temperature using 2/ZnO-NW: **2/ZnO-NW** was heated at 130, 140, 150, 160, 170, 180, 190, and 200 °C for 10 min on a hotplate. After cooling to room temperature, **5Cl** was introduced to **2'/ZnO-NW** via Huisgen cycloaddition using the same procedure described in Section 6.4. The resulting samples, **5Cl-2'/ZnO-NW**, were used for SEM-EDS analysis. The plot of the normalized values relative to the initial level at each temperature $(Cl/P)/(Cl/P)_0$ is shown in Fig. S11.

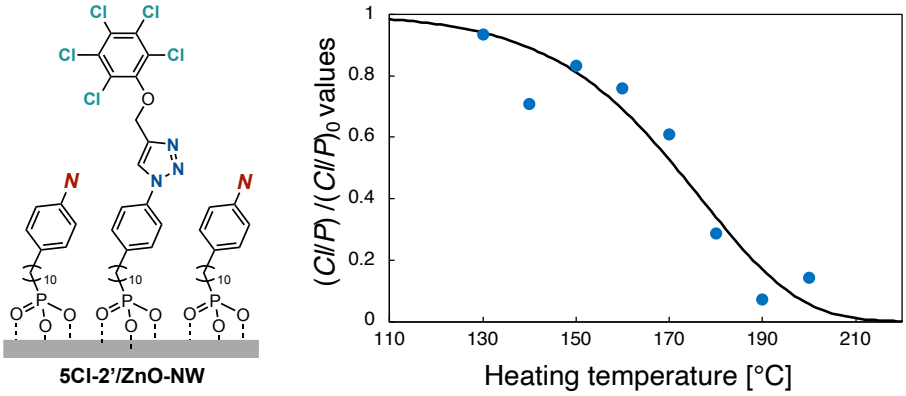

Fig. S11 Calibration curve obtained by fitting the measured $(Cl/P)/(Cl/P)_0$ values of **5Cl-2'/ZnO-NW**, based on SEM-EDS analysis (heating temperature: 130, 140, 150, 160, 170, 180, 190, and 200 °C for 10 min).

6.10. Preparation of calibration curve: The normalized value relative to the initial level at each temperature, $(Cl/P)/(Cl/P)_0$ calculated by SEM-EDS analysis is theoretically comparable to the azido-decomposition ratio ($[N_3]/[N_3]_0$, in first-order reaction) determined by FT-IR measurements. Thus, the calibration curve shown in Fig. S11 was constructed as follows (eqn. S2):

$$\frac{(Cl/P)}{(Cl/P)_0} = \frac{(N3)}{(N3)_0} = \exp(-kt) = \exp\left\{-A\exp\left(-\frac{E_a}{RT}\right)\cdot t\right\} \qquad \text{(S2)}$$

where k is reaction rate constant based on Arrhenius equation (eqn. S1), E_a is the activation energy, R is the universal gas constant, T is temperature, A is the pre-exponential factor, and t is the heating time (10 min). The calibration curves for **5Cl-1'/ZnO-NW** and **5Cl-2'/ZnO-NW** are shown in eqn. S3 and S4, respectively.

$$\frac{(Cl/P)}{(Cl/P)_0} = \exp\left\{-3.26\times10^{15}\exp\left(-\frac{1.81\times10^4}{T}\right)\right\} \qquad \text{(S3)}$$

$$\frac{(Cl/P)}{(Cl/P)_0} = \exp\left\{-1.25 \times 10^9 \exp\left(-\frac{9.60 \times 10^3}{T}\right)\right\} \qquad \text{(S4)}$$

The $(Cl/P)/(Cl/P)_0$ values were obtained through SEM-EDS measurements (three times at each temperature). The average of the three values was plotted against temperature to provide a calibration curve (Fig. S10).

The differences between the measured $(Cl/P)/(Cl/P)_0$ values and the calibration curve at each temperature is defined as $\Delta(Cl/P)/(Cl/P)_0$. Assuming that $\Delta(Cl/P)/(Cl/P)_0$ exhibits no temperature-dependence and follows a normal distribution, $\Delta(Cl/P)/(Cl/P)_0$ has a mean of –0.0269 and a standard deviation of 0.110. The 90% confidence interval for $\Delta(Cl/P)/(Cl/P)_0$ ranges from 0.154 on the positive side to 0.208 on the negative side relative to the calibration curve.

Based on the above consideration, the calibration curve was vertically shifted by the confidence interval (+0.154 to –0.208), generating two additional curves shown as gray curves in Fig. S12. We adopted the region enclosed by the two gray curves as an uncertainty range of the calibration curve for calculating the heating temperature. Representative raw data of each SEM-EDS measurement are shown in Fig. S13. All data with outliers removed according to box-and-whisker diagram are listed in Table S1–S3.

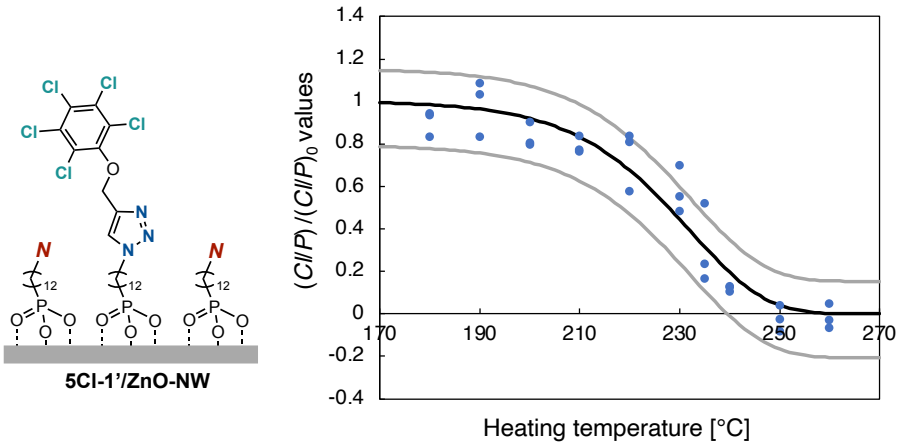

Fig. S12 Calibration curve obtained by fitting the measured $(Cl/P)/(Cl/P)_0$ values of **5Cl-1'/ZnO-NW** based on SEM-EDS analysis. The region enclosed by gray two curves represents the estimated uncertainty range of the calibration curve.

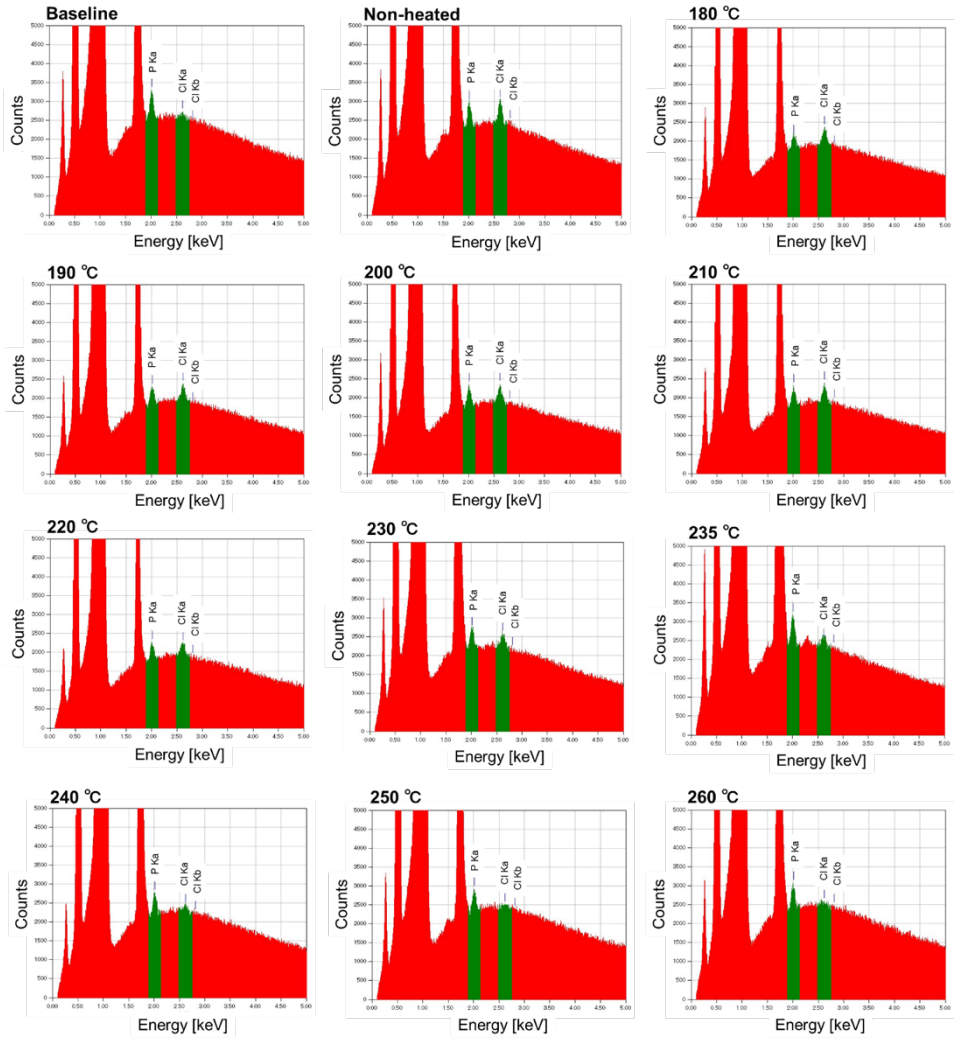

Fig. S13 Representative raw data of SEM-EDS analysis of 1-dodecylphosphonic acid-modified ZnO NWs, non-heated **5Cl-1/ZnO-NW**, and **5Cl-1'/ZnO-NW** (heated at 180, 190, 200, 210, 220, 230, 235, 240, 250, and 260 °C).

Table S1 SEM-EDS data of 1-dodecylphosphonic acid-modified ZnO NWs.

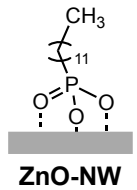 ZnO-NW	Run	*Cl* (intensity)	*P* (intensity)	*Cl*/P
	1	1133	5635	0.2011
	2	1388	5888	0.2358
	3	1341	5868	0.2285
	Average	-	-	0.2218

Table S2 SEM-EDS data of non-heated **5Cl-1/ZnO-NW**.

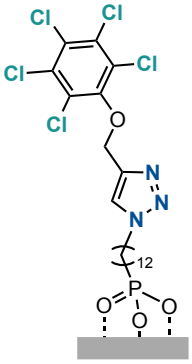 5Cl-1/ZnO-NW	Run	*Cl* (intensity)	*P* (intensity)	*Cl*/*P*	*Cl*/*P*[a]
	1	5378	4573	1.176	0.9543
	2	5450	3755	1.451	1.230
	3	5365	4169	1.287	1.065
	4	5425	4136	1.312	1.090
	5	5635	4052	1.391	1.169
	6	5143	4384	1.173	0.9515
	7	6208	3998	1.553	1.331
	Average	-	-	-	1.113

[a] Subtracted the data of 1-dodecylphosphonic acid-modified ZnO NWs.

Table S3 SEM-EDS data of **5Cl-1'/ZnO-NW** (heated at 180, 190, 200, 210, 220, 230, 235, 240, 250, and 260 °C; measured three times at each temperature).

	Temp. [°C]	*Cl* (intensity)	*P* (intensity)	*Cl*/*P*	*Cl*/*P*[a]	*Cl*/*P*[b]
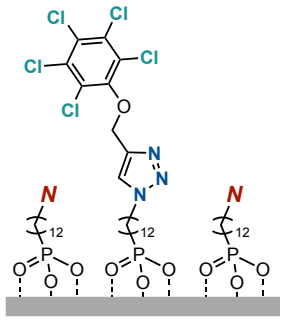 **5Cl-1'/ZnO-NW**	180	4096	3292	1.244	1.023	0.9188
		3185	2821	1.129	0.9071	0.8151
		3862	3117	1.239	1.017	0.9140
	190	4032	3000	1.344	1.122	1.008
		3368	2990	1.126	0.9043	0.8126
		3749	2678	1.400	1.178	1.059
	200	4108	3786	1.085	0.8633	0.7757
		4209	3497	1.204	0.9819	0.8823
		3964	3616	1.096	0.8743	0.7856
	210	3727	3544	1.052	0.8301	0.7458
		5531	4890	1.131	0.9095	0.8172
		4849	4563	1.063	0.8409	0.7555
	220	3424	3029	1.130	0.9085	0.8163
		4567	5387	0.8478	0.6260	0.5625
		5015	4564	1.099	0.8770	0.7880
	230	3924	4006	0.9797	0.7579	0.6810
		2917	3545	0.8229	0.6011	0.5401
		2706	3616	0.7483	0.5266	0.4731
	235	2355	4936	0.4771	0.2553	0.2294
		2799	3547	0.7892	0.5674	0.5098
		2564	6334	0.4048	0.1831	0.1645
	240	1533	4247	0.3609	0.1391	0.1250
		1107	3046	0.3636	0.1418	0.1274
		1089	3240	0.3359	0.1141	0.1026
	250	914.0	3405	0.2685	0.0467	0.0419
		693.1	3522	0.1968	–0.0250	–0.0225
		562.3	4231	0.1329	–0.0889	–0.0799
	260	1275	4631	0.2753	0.0535	0.0481
		670.9	4351	0.1542	–0.0676	–0.0607
		944.6	4935	0.1914	–0.0304	–0.0273

[a] Subtracted the data of 1-dodecylphosphonic acid-modified ZnO NWs.

[b] Normalized by the data from non-heated **5Cl-1/ZnO-NW**.

With the same procedure for **5Cl-1'/ZnO-NW**, $\Delta(Cl/P)/(Cl/P)_0$ of **5Cl-2'/ZnO-NW** has a mean of –0.00987 and a standard deviation of 0.132. The 90% confidence interval for $\Delta(Cl/P)/(Cl/P)_0$ ranges from 0.208 on the positive side to 0.228 on the negative side relative to the calibration curve.

Based on the above consideration, the calibration curve was vertically shifted by the error margin (+0.208 to –0.228), generating two additional curves shown as gray curves in Fig. S14. We adopted the region enclosed by the two gray curves as an uncertainty range of the calibration curve for calculating the heating temperature. Representative raw data of each SEM-EDS measurement are shown in Fig. S15. All data with outliers removed according to box-and-whisker diagram are listed in Table S4 and S5. The values of 1-dodecylphosphonic acid-modified ZnO NWs shown in Table S1 were used for baseline correction.

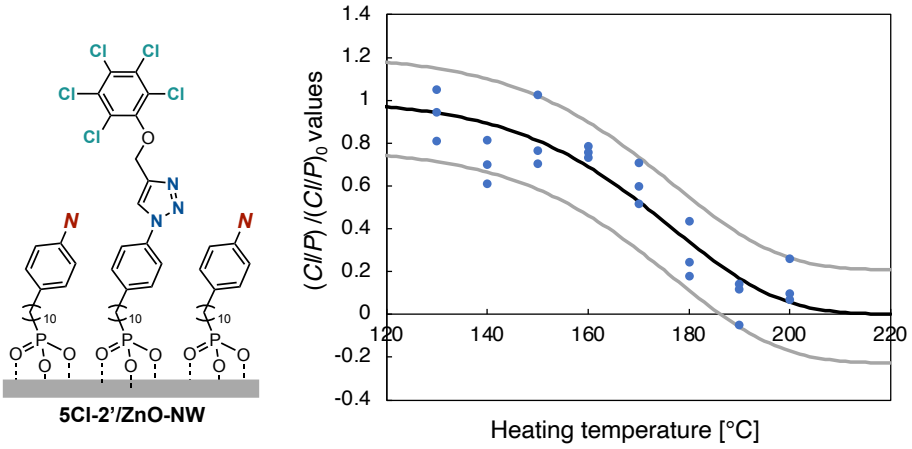

Fig. S14 Calibration curve obtained by fitting the measured $(Cl/P)/(Cl/P)_0$ values of **5Cl-2'/ZnO-NW** based on SEM-EDS analysis. The region enclosed by two gray curves represents the estimated uncertainty range of the calibration curve.

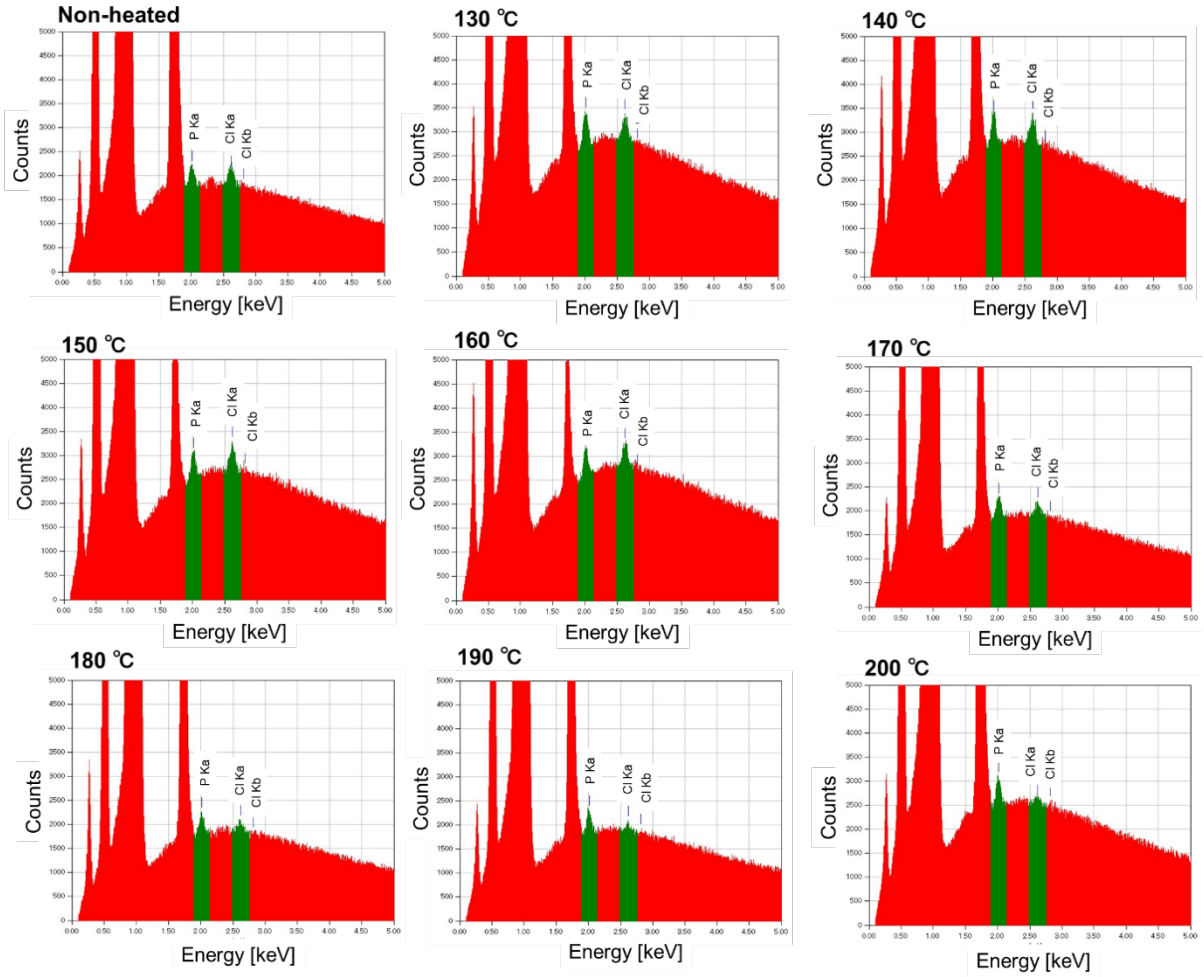

Fig. S15 Representative raw data of SEM-EDS analysis of non-heated **5Cl-2/ZnO-NW**, and **5Cl-2'/ZnO-NW** (heated at 130, 140, 150, 160, 170, 180, 190, and 200 °C).

Table S4 SEM-EDS data of non-heated **5Cl-2/ZnO-NW**.

	Run	*Cl* (intensity)	*P* (intensity)	*Cl*/*P*	*Cl*/*P*[a]
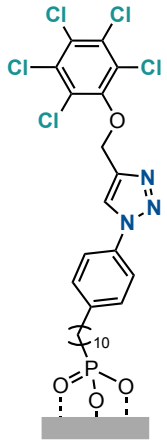	1	3740	2800	1.336	1.114
	2	3739	2922	1.280	1.058
	3	4274	3587	1.191	0.9697
	4	3712	3850	0.9642	0.7424
	5	3610	2860	1.263	1.041
	6	3904	3127	1.248	1.027
	7	3549	3910	0.9077	0.6859
	8	3590	3394	1.058	0.8360
	9	3298	2757	1.196	0.9747
5Cl-2/ZnO-NW	10	3636	3662	0.9930	0.7712
	Average	-	-	-	0.9219

[a] Subtracted the data of 1-dodecylphosphonic acid-modified ZnO NWs.

Table S5 SEM-EDS data of **5Cl-2'/ZnO-NW** (heated at 130, 140, 150, 160, 170, 180, 190, and 200 °C; measured three times at each temperature).

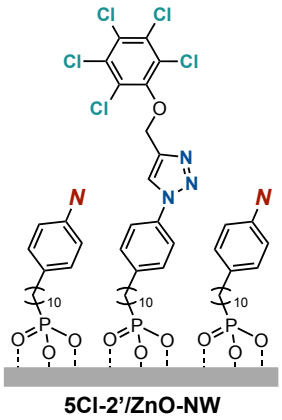

Temp. [°C]	*Cl* (intensity)	*P* (intensity)	*Cl*/*P*	*Cl*/*P*[a]	*Cl*/*P*[b]
130	5153	5307	0.9710	0.7492	0.8127
	5430	4558	1.191	0.9695	1.052
	4659	4264	1.093	0.8708	0.9445
140	4651	4785	0.9719	0.7501	0.8137
	4086	5191	0.7872	0.5654	0.6133
	4525	5209	0.8687	0.6469	0.7017
150	4709	4024	1.170	0.9484	1.029
	4063	4662	0.8715	0.6497	0.7048
	4303	4640	0.9274	0.7056	0.7653
160	4203	4555	0.9226	0.7008	0.7602
	4280	4766	0.8980	0.6762	0.7334
	4047	4280	0.9455	0.7237	0.7850
170	2434	3479	0.6996	0.4778	0.5183
	2904	3751	0.7741	0.5523	0.5990
	2700	3080	0.8766	0.6548	0.7102
180	1936	3105	0.6234	0.4016	0.4356
	1437	3716	0.3867	0.1649	0.1789
	1308	2917	0.4483	0.2266	0.2457
190	1199	3378	0.3550	0.1332	0.1445
	729	4082	0.1785	–0.0433	–0.0470
	1439	4358	0.3303	0.1085	0.1177
200	1160	4067	0.2853	0.0635	0.0689
	1846	3993	0.4622	0.2404	0.2608
	1474	4694	0.3140	0.0922	0.1000

[a] Subtracted the data of 1-dodecylphosphonic acid-modified ZnO NWs.

[b] Normalized by the data from non-heated **5Cl-2/ZnO-NW**.

6.11. Comparison between FT-IR and SEM-EDS analysis in thermal history: A calibration curve of azido-decomposition rate relative to heating temperature was prepared from the Arrhenius plot based on FT-IR analysis, and it was override on the calibration curve based on SEM-EDS analysis. With **1/ZnO-NW**, both curves showed good agreement, indicating that the azido-decomposition rate determined by SEM-EDS measurement was comparable to that determined directly by FT-IR measurement (Fig. S16a). In contrast, with **2/ZnO-NW**, both curves show a similar trend, but the different between the two curves was larger compared to those of **1/ZnO-NW**, especially at high temperatures (Fig. S17a). This is probably due to the aggregation of the surface aryl azide by π-π interactions, which retards the Huisgen cycloaddition due to steric hindrance.[10] This assumption is also supported by the lower azide conversion ratio of **2/ZnO-NW** in the surface Huisgen cycloaddition, compared to that of **1/ZnO-NW** (Fig. S16b and S17b).

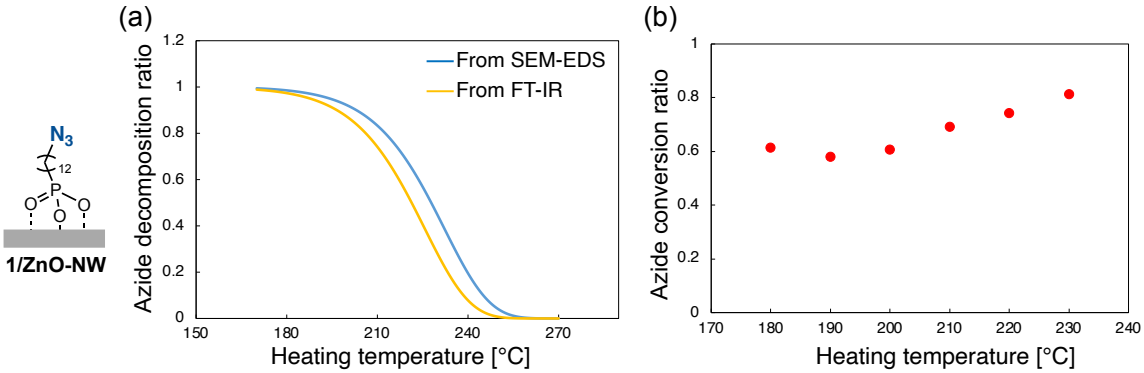

Fig. S16 (a) Comparison of azido-decomposition ratio between FT-IR and SEM-EDS analysis for **1/ZnO-NW**. (b) Azido-conversion ratio determined by FT-IR analysis at each heating temperature for **1/ZnO-NW** (At 235, 240, 250, and 260 °C, the peak corresponding to the azido group in the FT-IR spectra were too weak for calculating the conversion ratio).

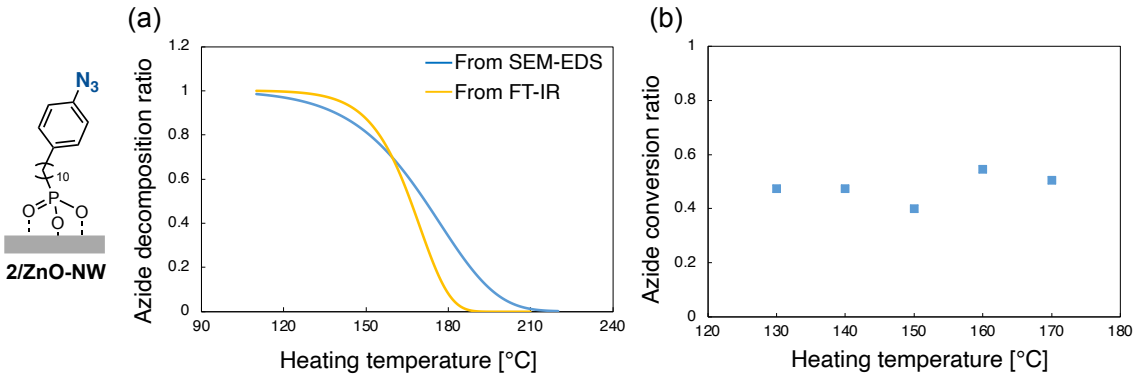

Fig. S17 (a) Comparison of azido-decomposition ratio between FT-IR and SEM-EDS analysis for **2/ZnO-NW**. (b) Azido-conversion ratio determined by FT-IR analysis at each heating temperature for **2/ZnO-NW** (At 180, 190, and 200 °C, the peak corresponding to the azido group in the FT-IR spectra were too weak for calculating the conversion ratio).

6.12. Fabrication of 1/ZnO-NW/Pt: Fig. S18 shows schematic procedure of **ZnO-NW/Pt**. Photoresist LOR3B and AZP1350 were employed to fabricate the microheater with lithography technology. Spin coating of LOR3B was performed on surface oxide Si substrates at 500 rpm for 5 seconds followed by 2500 rpm for 45 seconds. Thermal baking procedure was performed at 190 °C for 5 min. Subsequently, spin coating of AZP1350 was performed on surface oxide Si substrates at 500 rpm for 5 seconds followed by 2000 rpm for 60 seconds. Thermal baking procedure was performed at 100 °C for 140 s, and then the patterning process was carried out using a photolithography machine (Heidelberg Instruments μPG 101 UOW1) at an energy of 40 mW. Then, to enhance the adhesion between a SiO_2 substrate and Pt, a Ti thin layer was deposited on the patterned substrate by RF sputtering at a power of 100 W and an Ar pressure of 0.3 Pa with the thickness of ~3 nm. Subsequently, Pt was deposited on the substrates with the thickness of 200 nm (RF at 50 W). A lift-off process was performed using DMF. Pt square areas were protected with carbon tape to avoid being covered with ZnO NWs. A Ti thin layer was deposited on the substrates with the thickness of ~20 nm (RF at 100 W) to enhance the adhesion between the substrate and ZnO. Subsequently, ZnO was deposited on the substrates with the thickness of ~6 nm (RF at 50 W) as a seed layer. ZnO NWs were grown using the hydrothermal method.[6] 5.5 mM Polyethylenimine (Mw ~2,000, 50 wt.% in H_2O), 25 mM hexamethylenetetramine, and 25 mM $Zn(NO_3)_2 \cdot 6H_2O$ were dissolved sequentially in distilled water (200 mL). The pre-prepared substrate was dipped into the solution and maintained at 80 °C for 16 h. After growth, the carbon-tape mask was removed, and the samples were rinsed with distilled water. Then the as-grown ZnO NWs were annealed at 400 °C in the air for 1 h to give **ZnO-NW/Pt**. The azide-modified **1/ZnO-NW/Pt** was prepared from **1** and **ZnO-NW/Pt** using the same procedure described in Section 6.2.

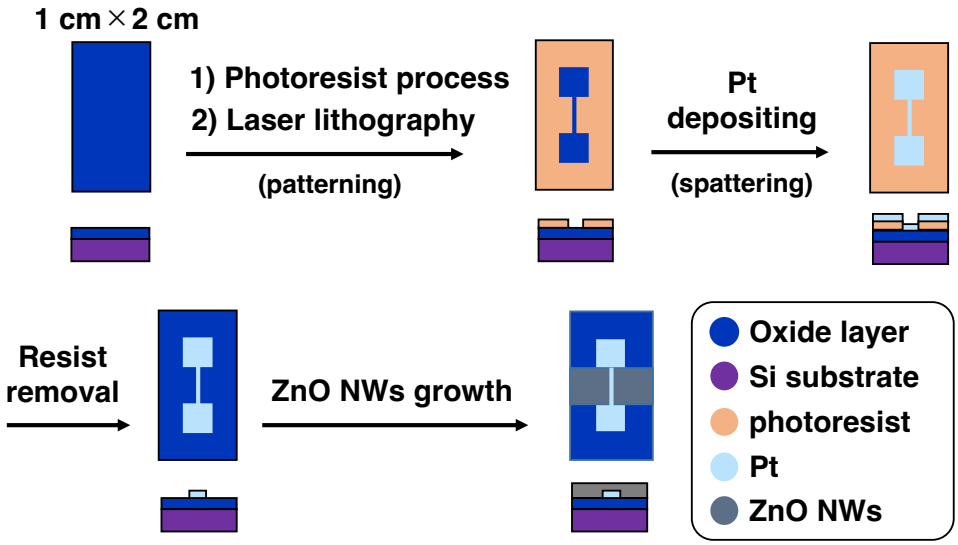

Fig. S18 Preparation procedure of **ZnO-NW/Pt**.

6.13. Local Joule heating of 1/ZnO-NW/Pt: The square Pt area of **1/ZnO-NW/Pt** was connected to a power supply using silver paste (Fig. S19a). A voltage of 80 V was applied for 10 min for Joule heating with **1/ZnO-NW/Pt** (Fig. S19b). After cooling to room temperature, **5Cl** was introduced via Huisgen cycloaddition using the same procedure described in Section 6.4., excepting for washing with DMSO only to prevent the silver paste from dissolving out. The resulting **5Cl-1'/ZnO-NW/Pt** was analyzed by SEM-EDS measurement in 3 μm × 4 μm range from the edge of Pt heating site (Fig. S19c). Since all experiments were conducted on a single substrate, the Cl intensity relative to that of the initial value (denoted as Cl/Cl_0) was directly used without normalization with the P value derived from the phosphonic acid anchor. Each measurement was conducted at distance of 30, 60, 90, 180, 270, 360, 450, 540, and 720 μm from the edge of Pt heating site (Fig. S20a). The temperature distribution was calculated with the calibration curve obtained in eqn. S3, and its uncertainty was quantified based on the uncertainty range shown in Fig. S12 (Fig. S20b). Raw data of each measurement are shown in Fig. S21. All data are listed in Table S6–S8.

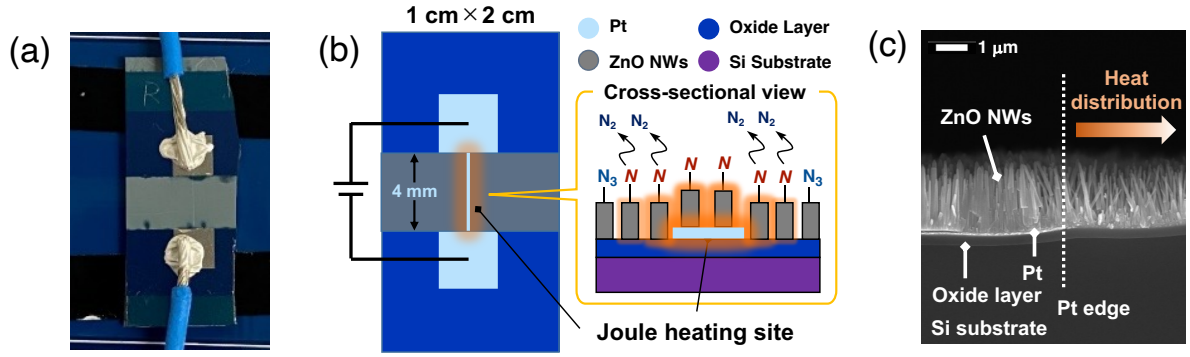

Fig. S19 (a) Photograph and (b) Schematic of **1/ZnO-NW/Pt**. The Pt heating site has dimensions of 4 mm length × 10 μm width × 200 nm depth. (c) Cross-sectional SEM image of **ZnO-NW/Pt** before SAM preparation with **1**. Heat distribution was measured from the Pt edge.

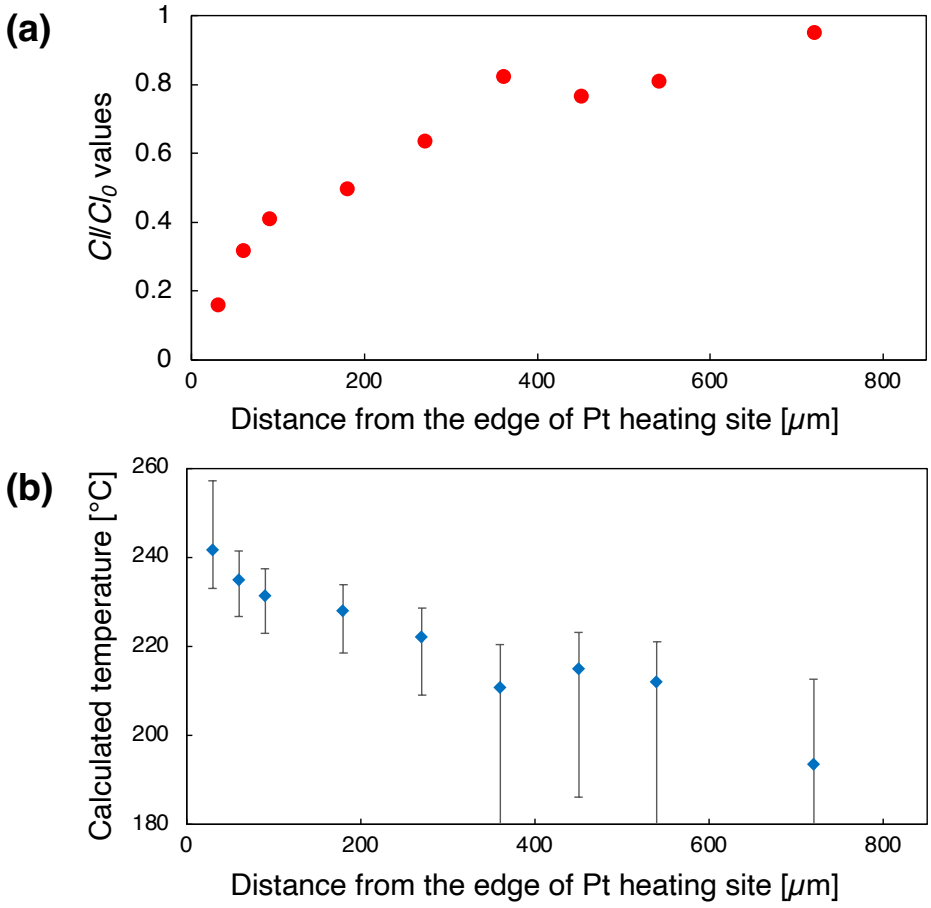

Fig. S20 (a) EDS signal intensity and (b) temperature plotted as a function of distance from the edge of Pt heating site in **5Cl-1'/ZnO-NW/Pt** (distance: 30, 60, 90, 180, 270, 360, 450, 540, and 720 μm).

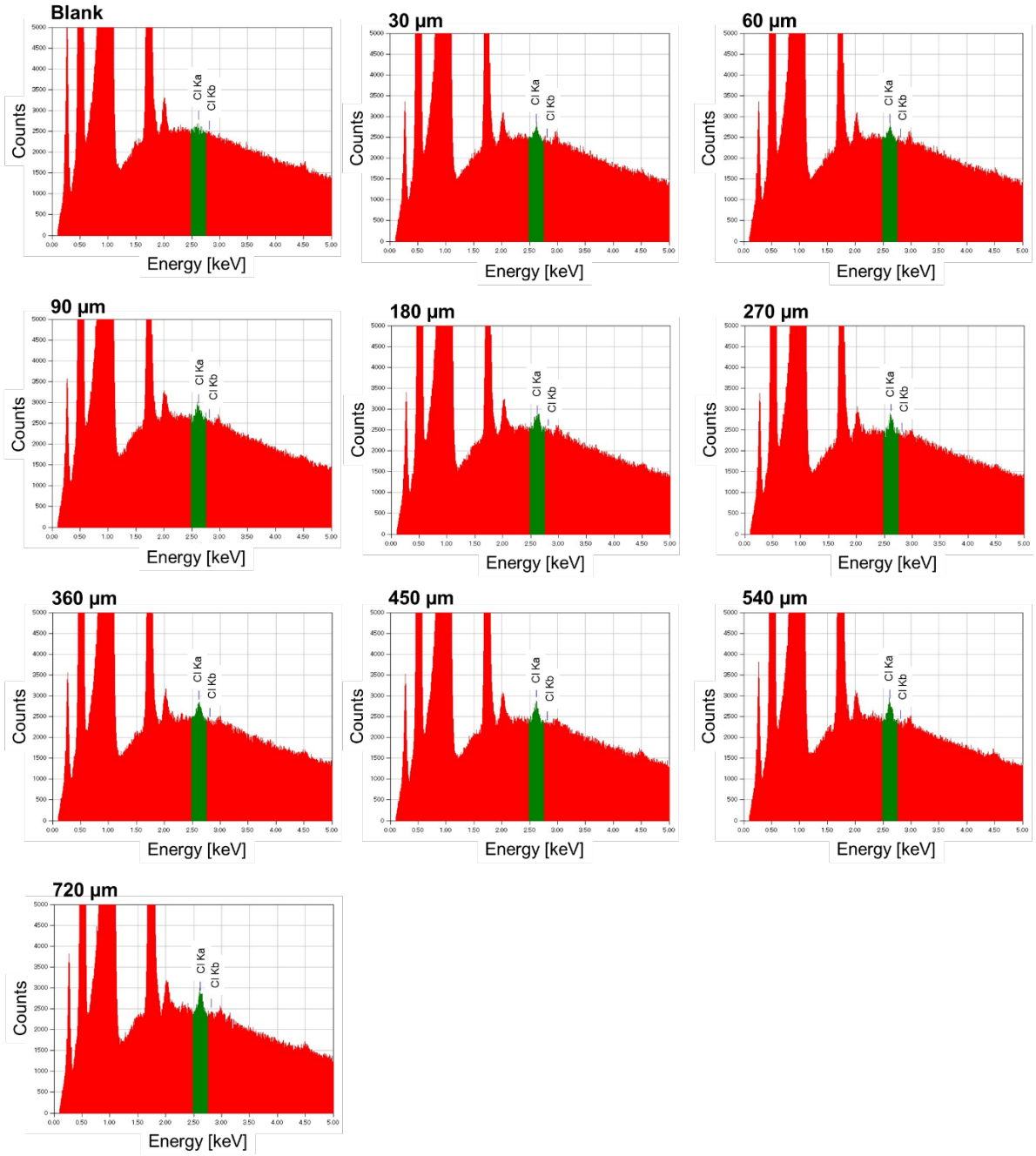

Fig. S21 Raw data of SEM-EDS analysis of 1-dodecylphosphonic acid-modified **ZnO-NW/Pt**, non-heated **5Cl-1/ZnO-NW/Pt**, and **5Cl-1'/ZnO-NW/Pt** (at distance of 30, 60, 90, 180, 270, 360, 450, 540, and 720 µm from the edge of Pt heating site).

Table S6 SEM-EDS data of 1-dodecylphosphonic acid-modified **ZnO-NW/Pt**.

	Run	*Cl* (intensity)
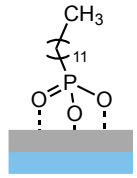 **ZnO-NW/Pt**	1	1061
	2	1183
	3	798
	4	1331
	Average	1093

Table S7 SEM-EDS data of non-heated **5Cl-1/ZnO-NW/Pt**.

	Run	*Cl* (intensity)	*Cl* (intensity)[a]
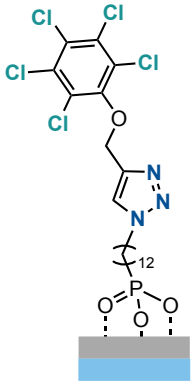 **5Cl-1/ZnO-NW/Pt**	1	3550	2457
	2	4339	3246
	Average	-	2851

[a] Subtracted the data of 1-dodecylphosphonic acid-modified **ZnO-NW/Pt**.

Table S8 SEM-EDS data of **5Cl-1'/ZnO-NW/Pt** from the edge of Pt heating site.

	Distance [μm]	*Cl* (intensity)	*Cl* (intensity)[a]	Cl/Cl_0 (intensity)[b]
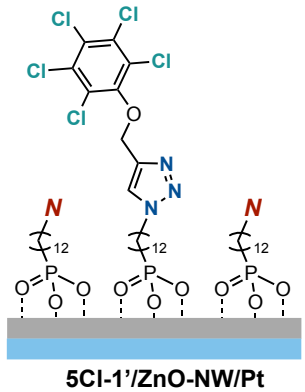 **5Cl-1'/ZnO-NW/Pt**	30	1549	456	0.160
	60	2001	908	0.318
	90	2260	1167	0.4094
	180	2509	1417	0.4968
	270	2904	1811	0.6353
	360	3439	2346	0.8228
	450	3278	2185	0.7662
	540	3399	2307	0.8089
	720	3810	2717	0.9528

[a] Subtracted the data of 1-dodecylphosphonic acid-modified **ZnO-NW/Pt**.

[b] Normalized by the data from non-heated **5Cl-1/ZnO-NW/Pt**.

7. NMR Data

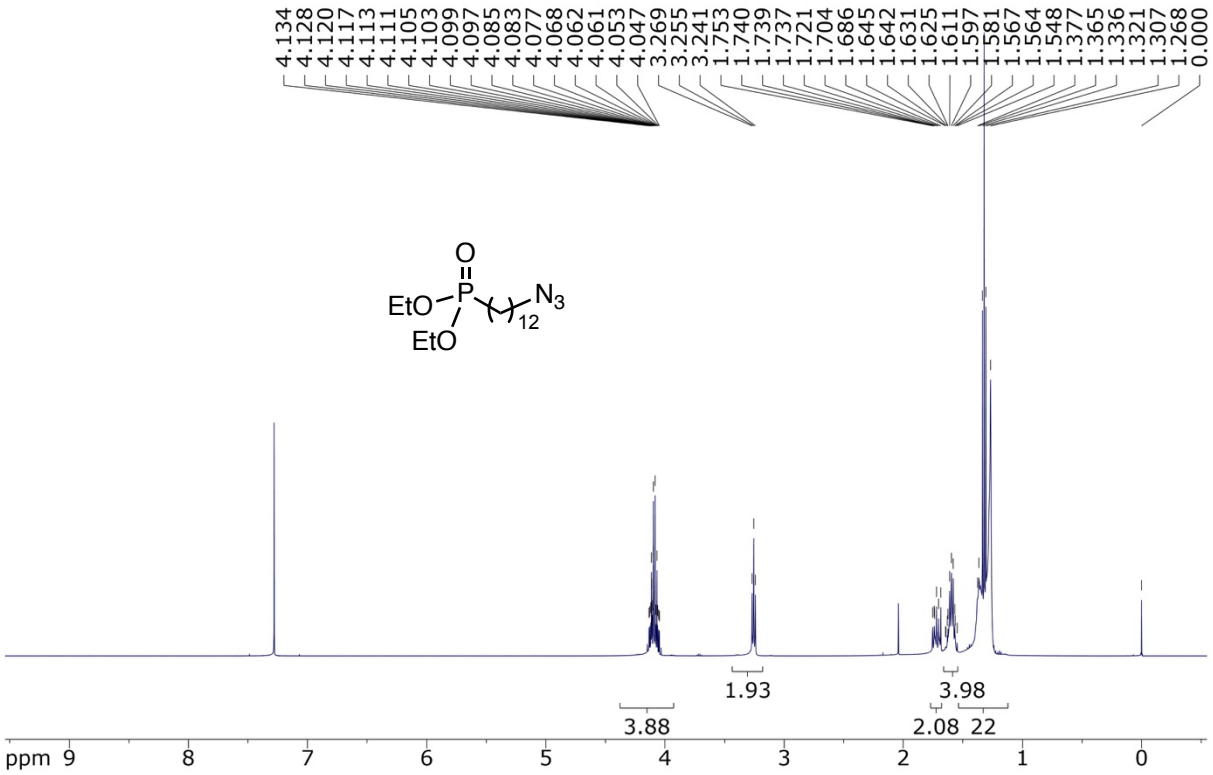

Fig. S22 ^{1}H NMR spectrum of compound **S1** (500 MHz, $CDCl_3$, r.t.).

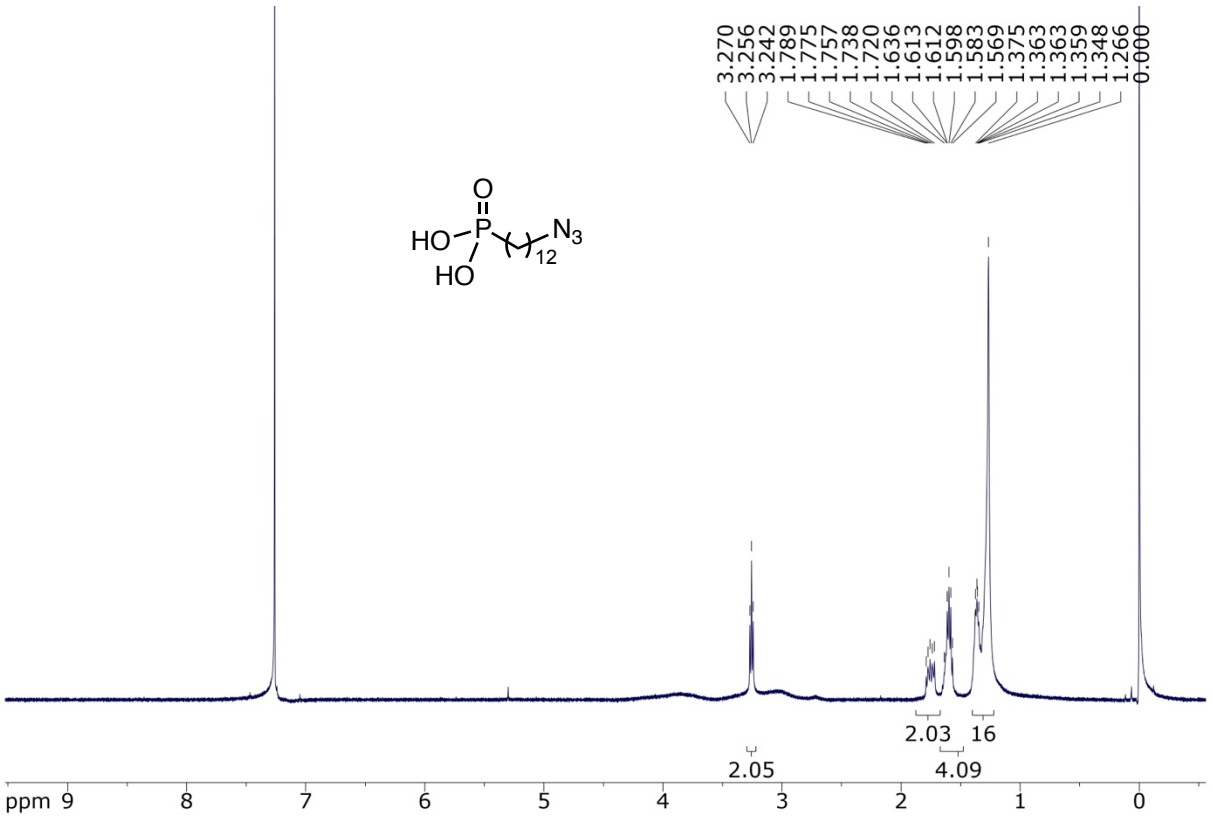

Fig. S23 ^{1}H NMR spectrum of compound **1** (500 MHz, $CDCl_3$, r.t.).

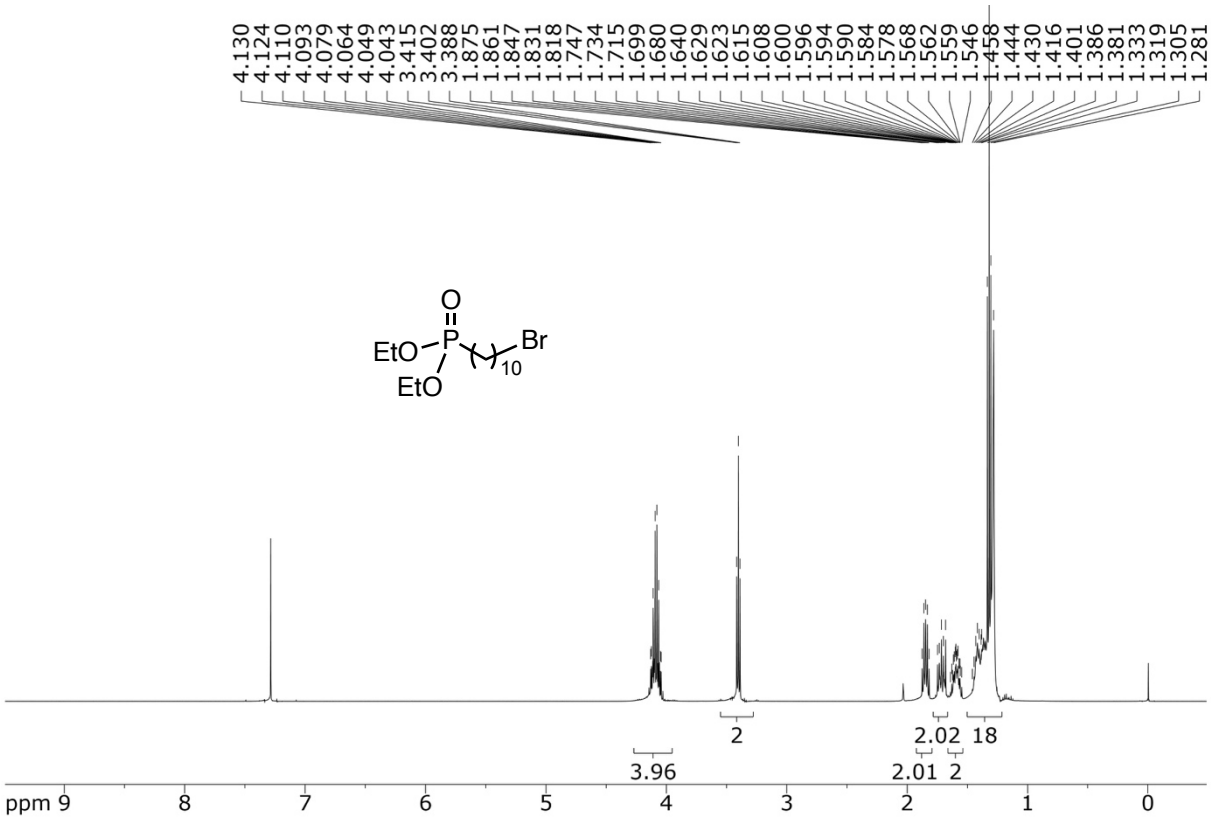

Fig. S24 ^{1}H NMR spectrum of compound **S2** (500 MHz, $CDCl_3$, r.t.).

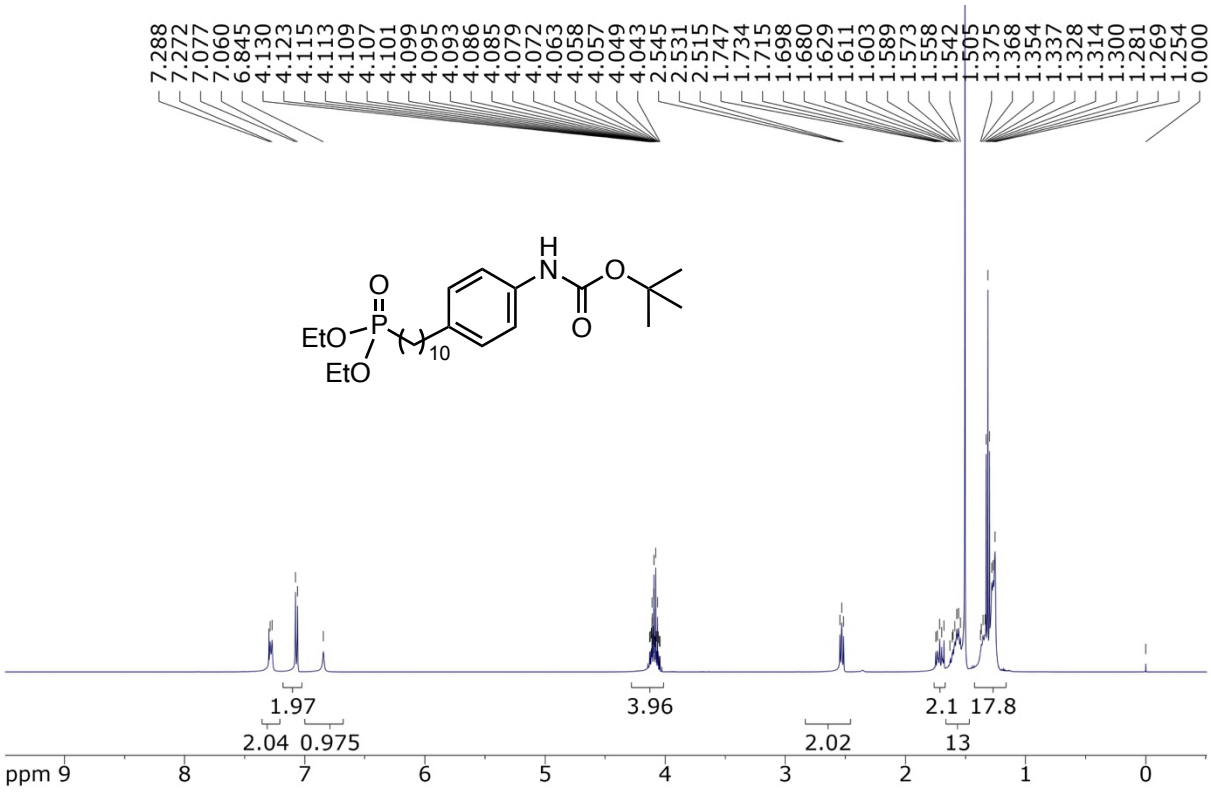

Fig. S25 ^{1}H NMR spectrum of compound **S3** (500 MHz, $CDCl_3$, r.t.).

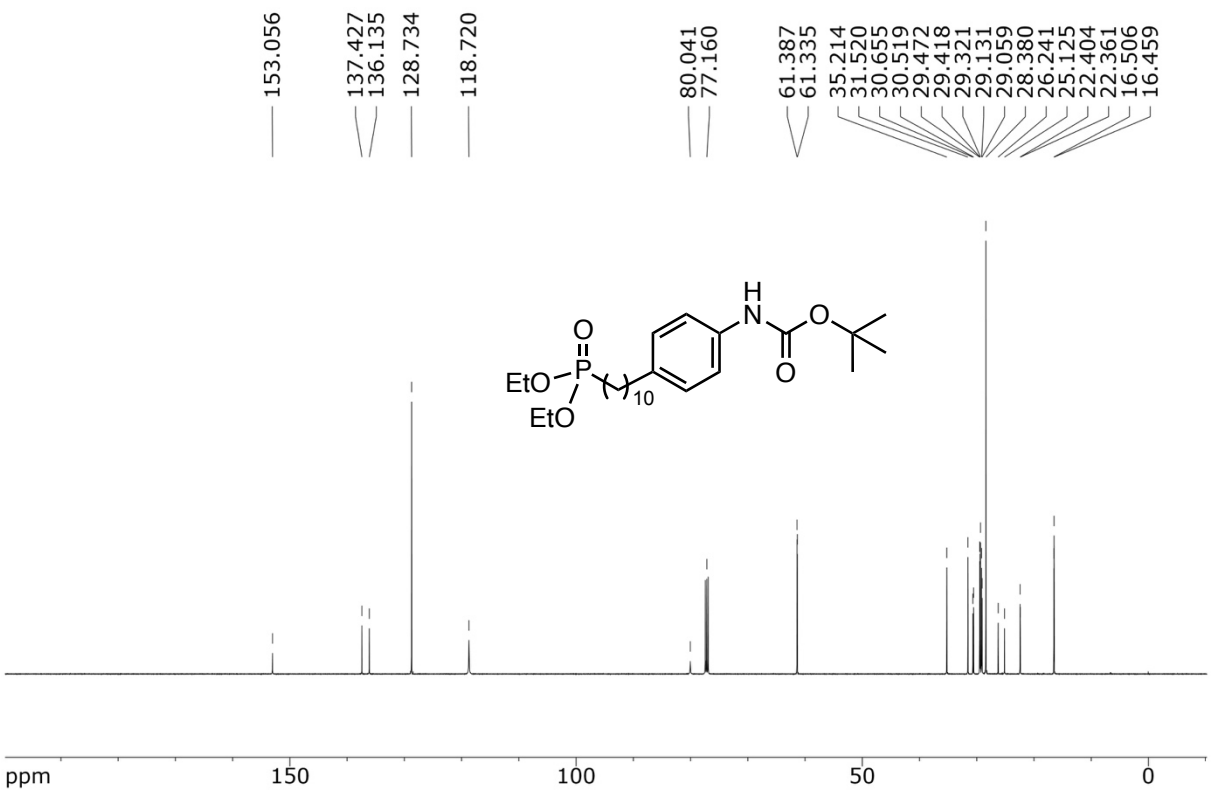

Fig. S26 ^{13}C NMR spectrum of compound **S3** (126 MHz, $CDCl_3$, r.t.).

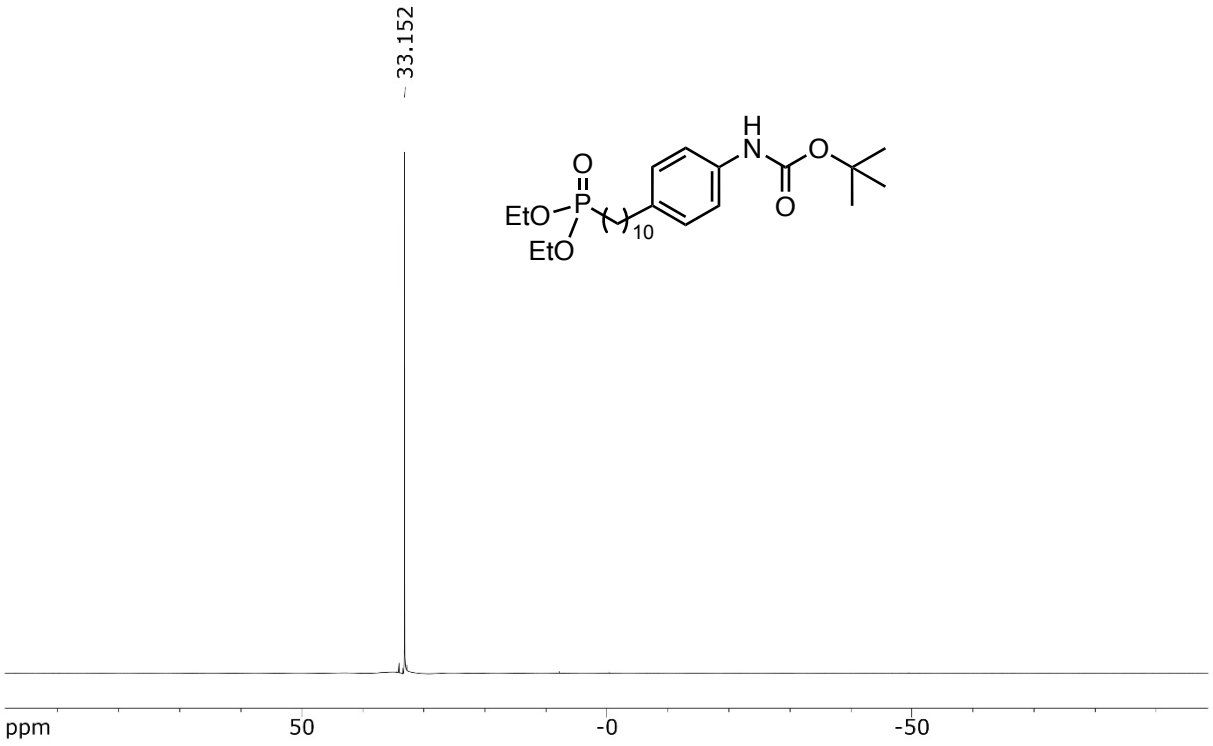

Fig. S27 ^{31}P NMR spectrum of compound **S3** (202 MHz, $CDCl_3$, r.t.).

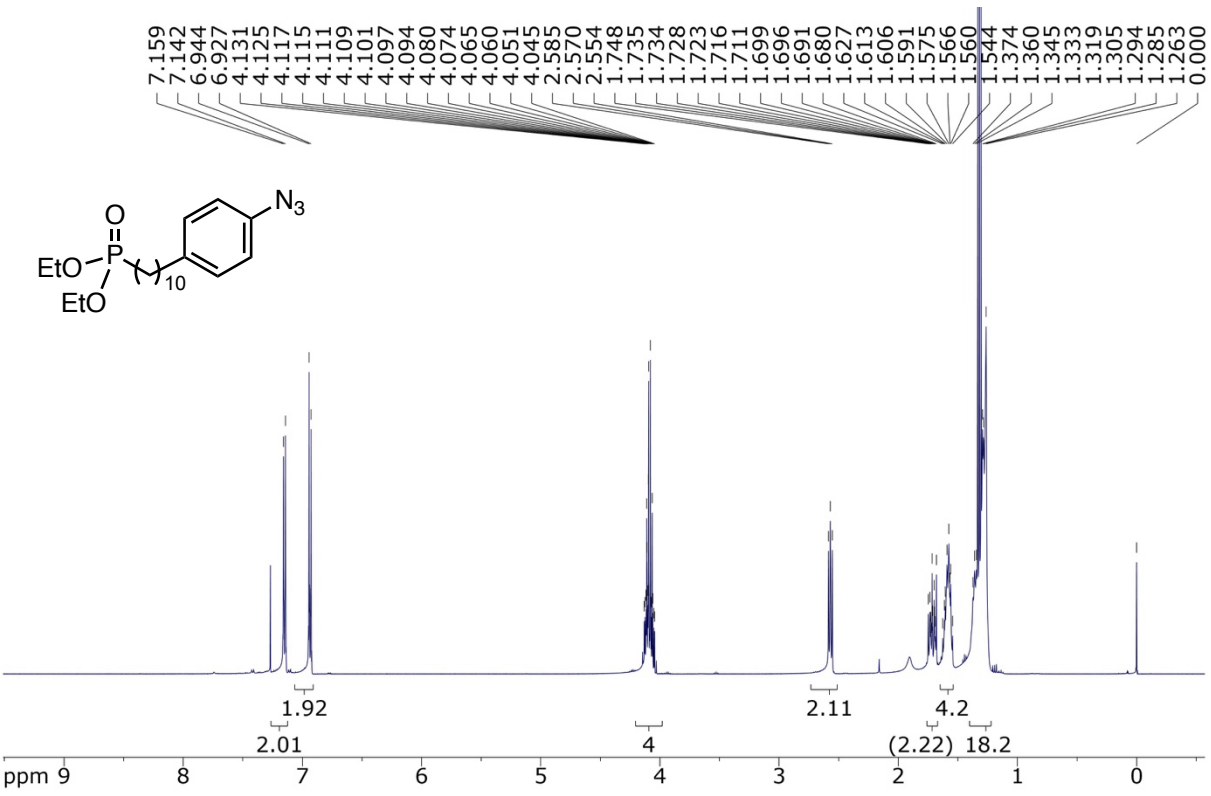

Fig. S28 ^{1}H NMR spectrum of compound **S4** (500 MHz, $CDCl_3$, r.t.).

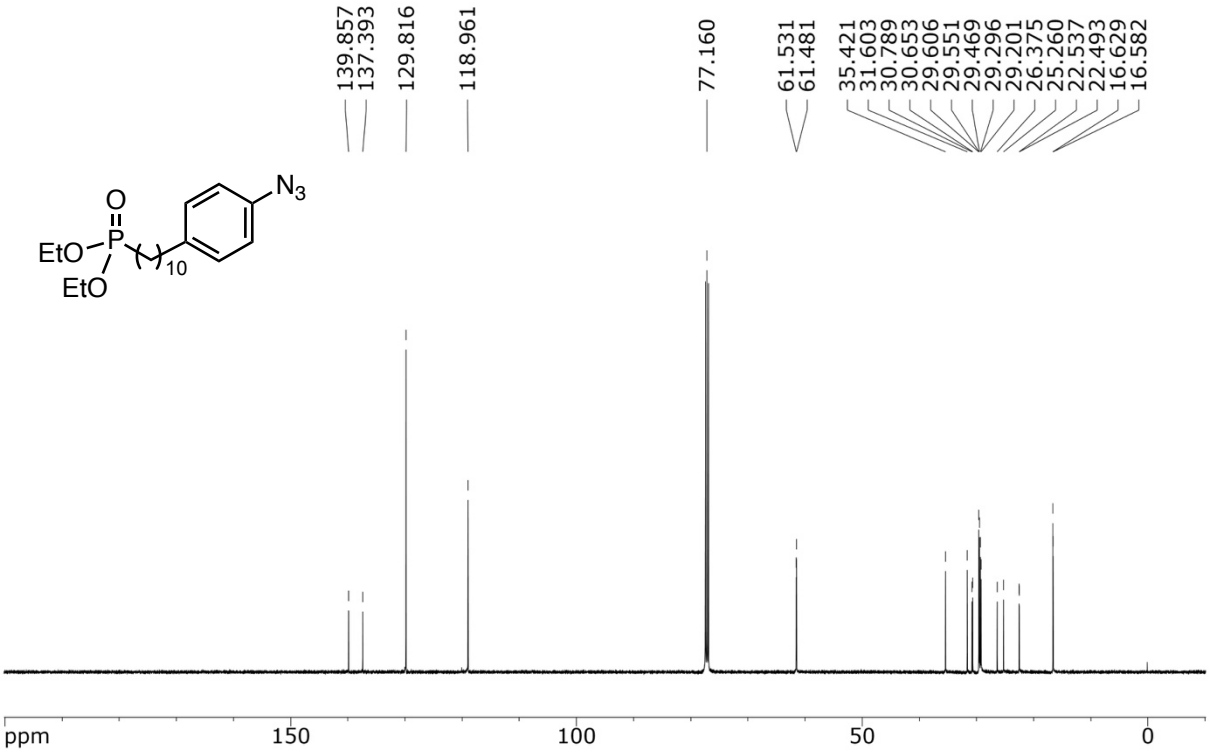

Fig. S29 ^{13}C NMR spectrum of compound **S4** (126 MHz, $CDCl_3$, r.t.).

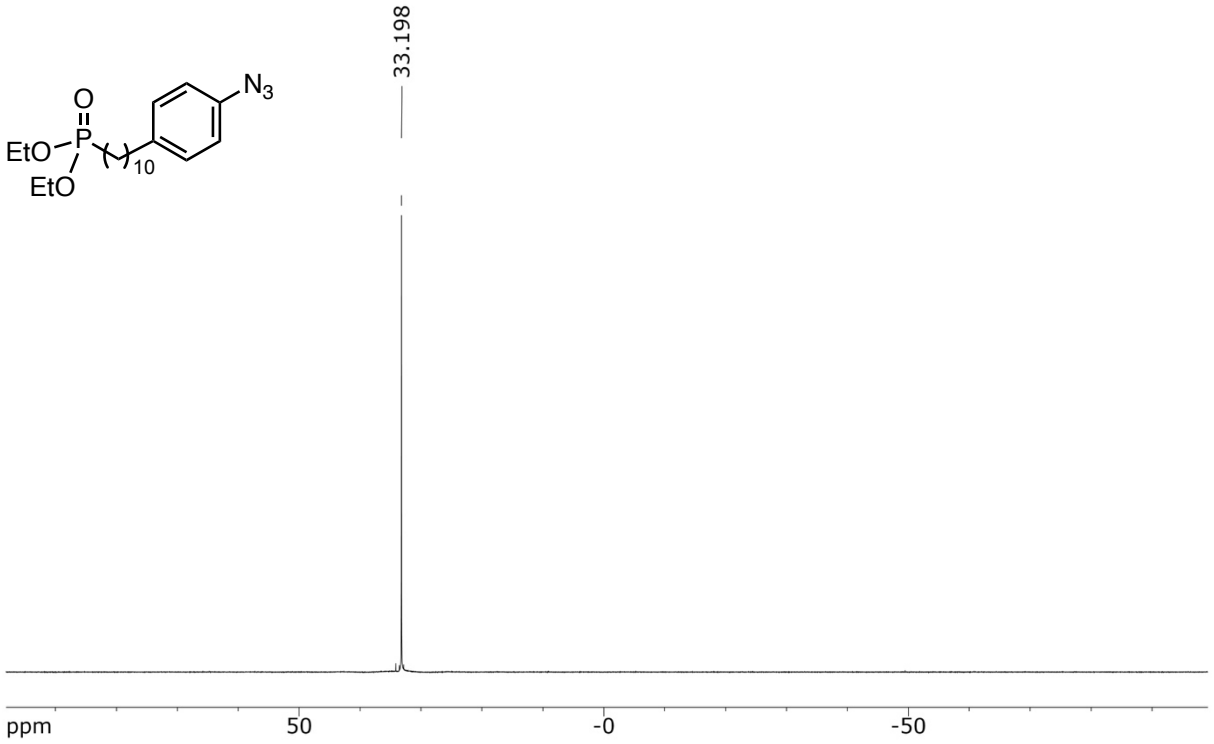

Fig. S30 ^{31}P NMR spectrum of compound **S4** (202 MHz, $CDCl_3$, r.t.).

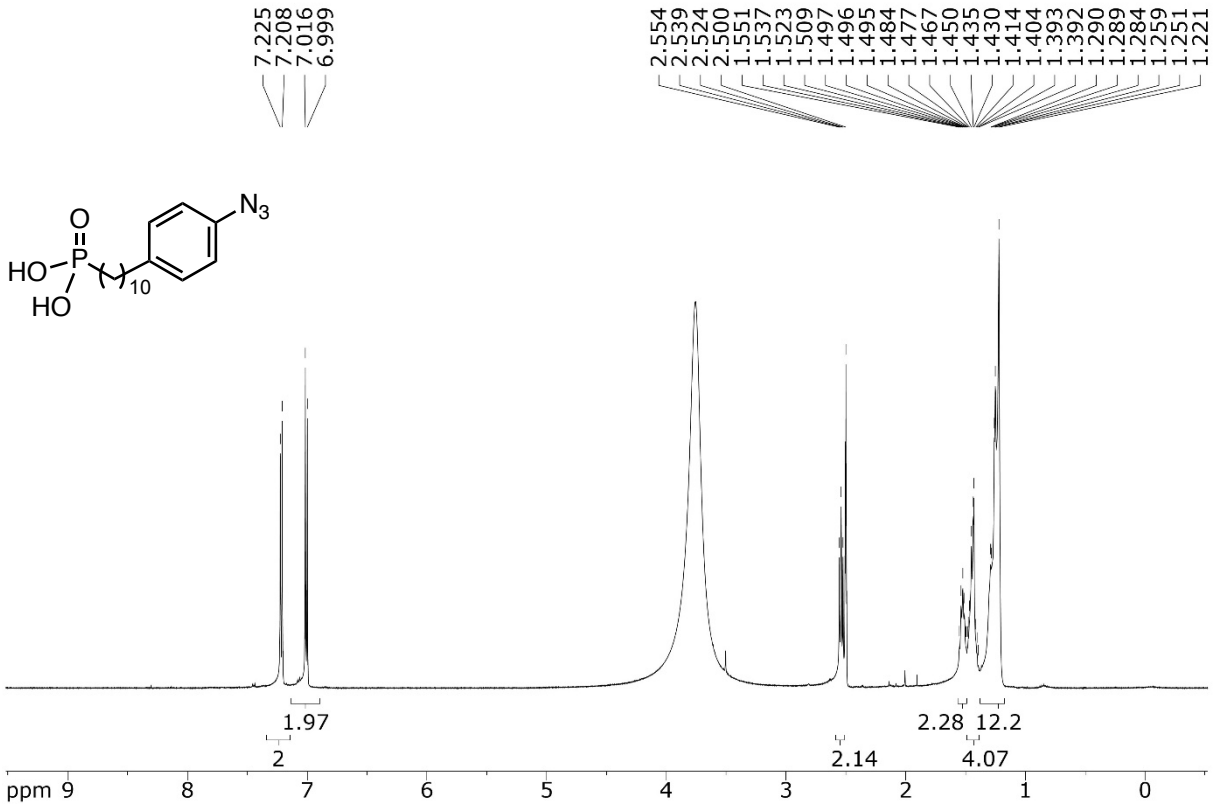

Fig. S31 ^{1}H NMR spectrum of compound **2** (500 MHz, DMSO-d_6, r.t.).

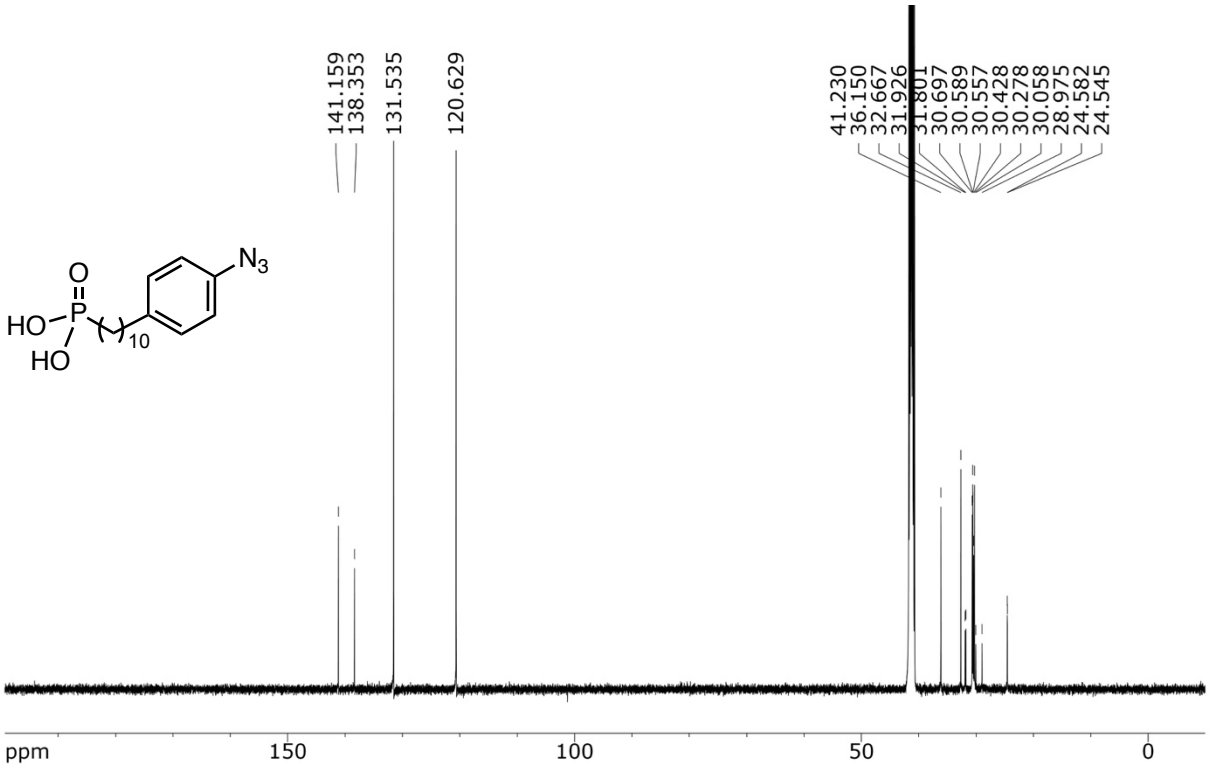

Fig. S32 ^{13}C NMR spectrum of compound **2** (126 MHz, DMSO-d_6, r.t.).

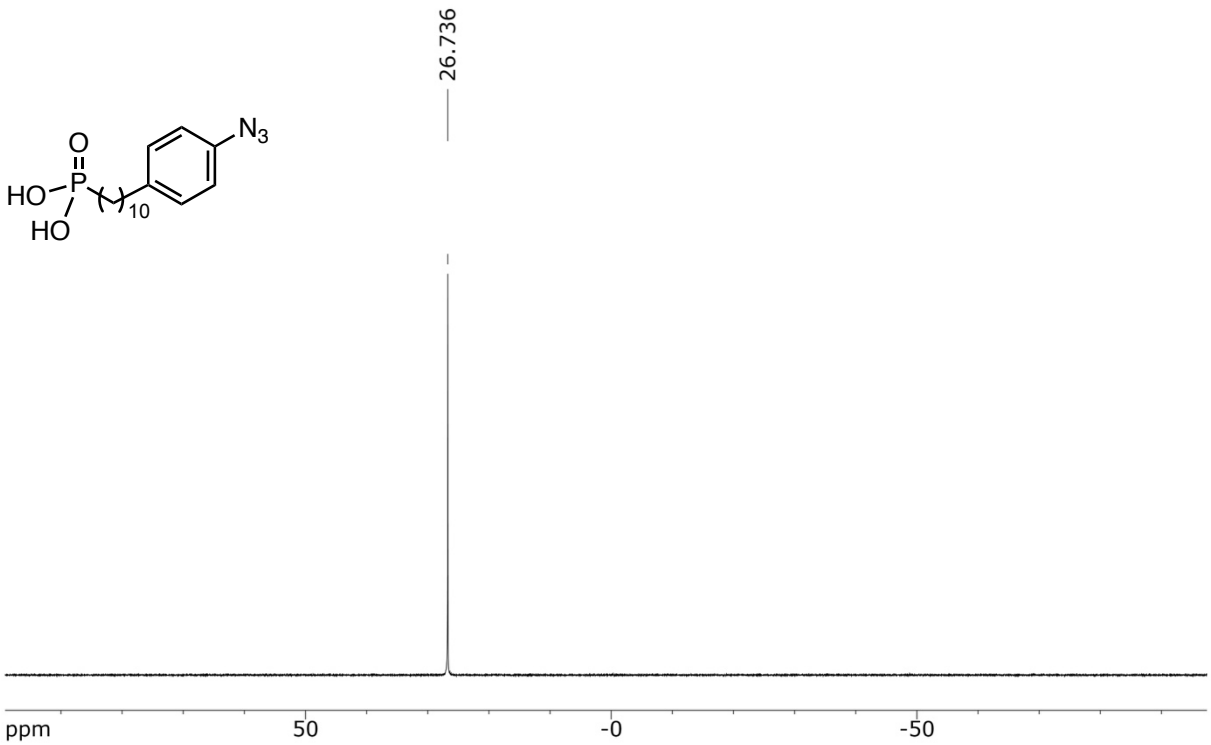

Fig. S33 ^{31}P NMR spectrum of compound **2** (202 MHz, DMSO-d_6, r.t.).

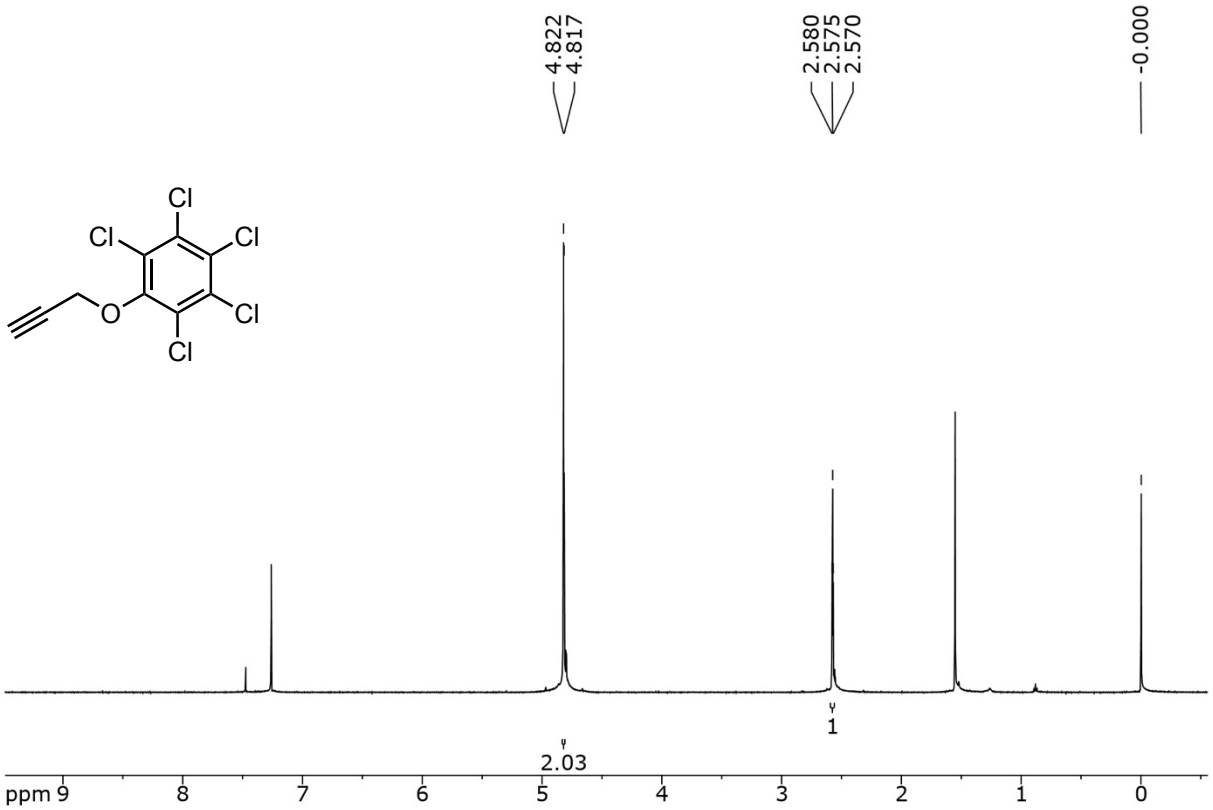

Fig. S34 ^{1}H NMR spectrum of compound **5Cl** (500 MHz, $CDCl_3$, r.t.).

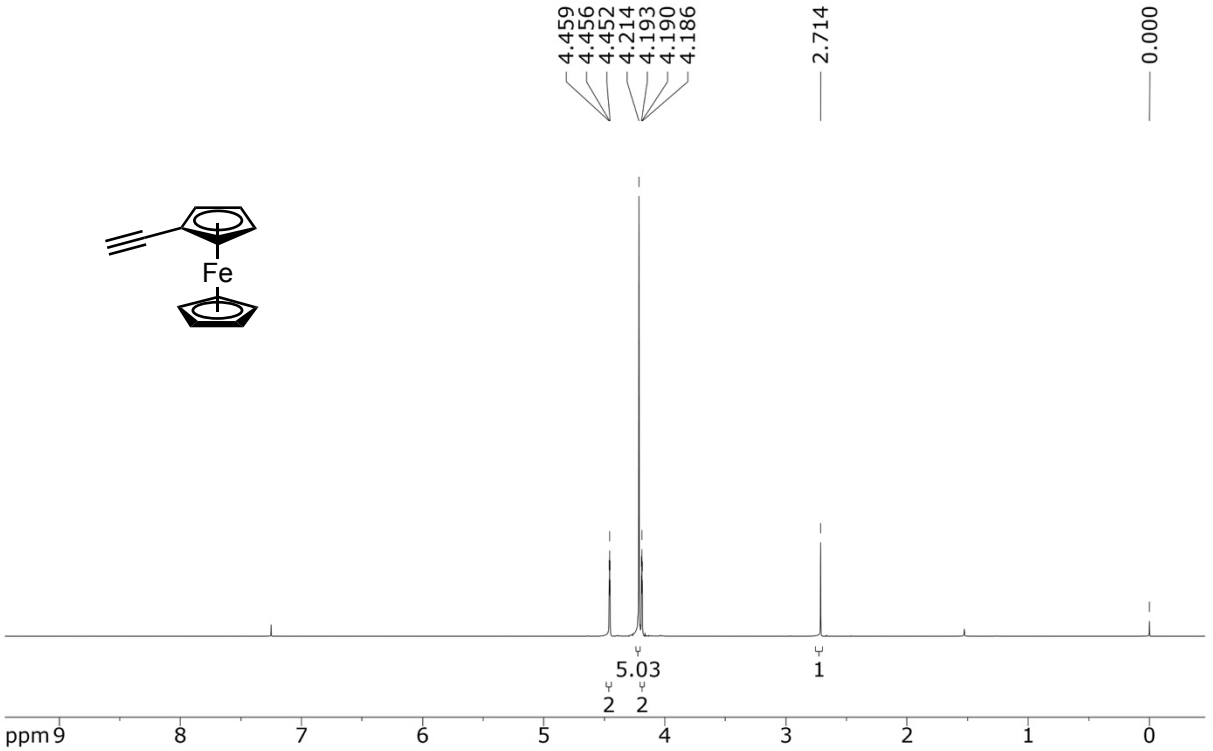

Fig. S35 ^{1}H NMR spectrum of compound **S5** (500 MHz, $CDCl_3$, r.t.).

8. References

1 A. B. Pangborn, M. A. Giardello, R. H. Grubbs, R. K. Rosen and F. J. Timmers, *Organometallics*, 1996, **15**, 1518–1520.

2 D. Toulemon, B. P. Pichon, C. Leuvrey, S. Zafeiratos, V. Papaefthimiou, X. Cattoën and S. Bégin-Colin, *Chem. Mater.*, 2013, **25**, 2849–2854.

3 M. Ikenberry, L. Peña, D. Wei, H. Wang, S. H. Bossmann, T. Wilke, D. Wang, V. R. Komreddy, D. P. Rillema and K. L. Hohn, *Green Chem*., 2014, **16**, 836–843.

4 D. Lasányi and G. Tolnai, *Org. Lett.*, 2019, **21**, 10057–10062.

5 L. Singh, D. Fontinha, D. Francisco, A. M. Mendes, M. Prudêncio and K. Singh, *J. Med. Chem.*, 2020, **63**, 1750–1762.

6 Y. Zhang, M. K. Ram, E. K. Stefanakos and D. Y. Goswami, *J. Nanomater.*, 2012, **2012**, 624520.

7 C. R. Harris, K. J. Millman, S. J. van der Walt, R. Gommers, P. Virtanen, D. Cournapeau, E. Wieser, J. Taylor, S. Berg, N. J. Smith, R. Kern, M. Picus, S. Hoyer, M. H. van Kerkwijk, M. Brett, A. Haldane, J. F. del Río, M. Wiebe, P. Peterson, P. Gérard-Marchant, K. Sheppard, T. Reddy, W. Weckesser, H. Abbasi, C. Gohlke and T. E. Oliphant, *Nature*, 2020, **585**, 357–362.

8 GitHub - ialxn/JEOL_eds: A python module to read binary data files by JEOL's Analysis Station software. https://github.com/ialxn/JEOL_eds (Accessed 5 Mar 2025).

9 R. Yamaguchi, T. Hosomi, M. Otani, K. Nagashima, T. Takahashi, G. Zhang, M. Kanai, H. Masai, J. Terao and T. Yanagida, *Langmuir*, 2021, **37**, 5172–5179.

10 Q.-C. Jiang, T. Iwai, M. Jo, T. Hosomi, T. Yanagida, K. Uchida, K. Hashimoto, T. Nakazono, Y. Yamada, A. Kobayashi, S. Takizawa, H. Masai and J. Terao, *Small*, 2024, **20**, 2403717.